Title

Deriving Global OH Abundance and Atmospheric Lifetimes for Long-Lived Gases: A Search for CH3CCl3 Alternatives.

Journal

Journal of Geophysical Research (JGR): Atmospheres, 122(21)

ISSN

2169-897X

Authors

Liang, Qing

Chipperfield, Martyn

Fleming, Eric

et al.

Publication Date

2017-11-16

DOI

10.1002/2017jd026926

Peer reviewed

Published in final edited form as:

J Geophys Res Atmos. 2017 November 16; 122(21): 11914–11933. doi:10.1002/2017jd026926.

Deriving Global OH Abundance and Atmospheric Lifetimes for Long-Lived Gases: A Search for CH_3CCl_3 Alternatives

Qing Liang[1,2], **Martyn P. Chipperfield**[3], **Eric L. Fleming**[1,4], **N. Luke Abraham**[5,6], **Peter Braesicke**[7], **James B. Burkholder**[8], **John S. Daniel**[8], **Sandip Dhomse**[3], **Paul J. Fraser**[9], **Steven C. Hardiman**[10], **Charles H. Jackman**[1], **Douglas E. Kinnison**[11], **Paul B. Krummel**[9], **Stephen A. Montzka**[12], **Olaf Morgenstern**[13], **Archie McCulloch**[14], **Jens Mühle**[15], **Paul A. Newman**[1], **Vladimir L. Orkin**[16], **Giovanni Pitari**[17], **Ronald G. Prinn**[18], **Matthew Rigby**[14], **Eugene Rozanov**[19,20], **Andrea Stenke**[19], **Fiona Tummon**[19], **Guus J. M. Velders**[21,22], **Daniele Visioni**[17], **Ray F. Weiss**[15]

[1]Atmospheric Chemistry and Dynamics Laboratory, NASA Goddard Space Flight Center, Greenbelt, Maryland, USA,

[2]Universities Space Research Association, GESTAR, Columbia, Maryland, USA

[3]National Centre for Earth Observation, School of Earth and Environment, University of Leeds, Leeds, UK

[4]Science Systems and Applications, Inc, Lanham, Maryland, USA

[5]National Centre for Atmospheric Science, Leeds, UK

[6]Department of Chemistry, University of Cambridge, Cambridge, UK

[7]Karlsruhe Institute of Technology, Karlsruhe, Germany

[8]Chemical Sciences Division, NOAA Earth System Research Laboratory, Boulder, Colorado, USA

[9]Climate Science Centre, CSIRO Oceans and Atmosphere, Aspendale, Vic, Australia

[10]Met Office Hadley Centre, Exeter, UK

[11]National Center for Atmospheric Research, Boulder, Colorado, USA

[12]Global Monitoring Division, NOAA Earth System Research Laboratory, Boulder, Colorado, USA

[13]National Institute of Water and Atmospheric Research, Wellington, New Zealand

[14]School of Chemistry, University of Bristol, Bristol, UK

[15]Scripps Institution of Oceanography, University of California, San Diego, La Jolla, California, USA

[16]National Institute of Standards and Technology, Gaithersburg, Maryland, USA

[17]Department of Physical and Chemical Sciences, Università dell'Aquila, L'Aquila, Italy

[18]Massachusetts Institute of Technology, Cambridge, Massachusetts, USA

Correspondence to: Q. Liang, qing.liang-1@nasa.gov.

[19]Institute for Atmospheric and Climate Science, ETH Zurich, Zurich, Switzerland

[20]Physikalisch-Meteorologisches Observatorium Davos World Radiation Centre, Davos Dorf, Switzerland

[21]National Institute for Public Health and the Environment, Bilthoven, Netherlands

[22]Institute for Marine and Atmospheric Research, Utrecht University, Utrecht, Netherlands

Abstract

An accurate estimate of global hydroxyl radical (OH) abundance is important for projections of air quality, climate, and stratospheric ozone recovery. As the atmospheric mixing ratios of methyl chloroform (CH_3CCl_3) (MCF), the commonly used OH reference gas, approaches zero, it is important to find alternative approaches to infer atmospheric OH abundance and variability. The lack of global bottom-up emission inventories is the primary obstacle in choosing a MCF alternative. We illustrate that global emissions of long-lived trace gases can be inferred from their observed mixing ratio differences between the Northern Hemisphere (NH) and Southern Hemisphere (SH), given realistic estimates of their NH-SH exchange time, the emission partitioning between the two hemispheres, and the NH versus SH OH abundance ratio. Using the observed long-term trend and emissions derived from the measured hemispheric gradient, the combination of HFC-32 (CH_2F_2), HFC-134a (CH_2FCF_3, HFC-152a (CH_3CHF_2), and HCFC-22 ($CHClF_2$), instead of a single gas, will be useful as a MCF alternative to infer global and hemispheric OH abundance and trace gas lifetimes. The primary assumption on which this multispecies approach relies is that the OH lifetimes can be estimated by scaling the thermal reaction rates of a reference gas at 272 K on global and hemispheric scales. Thus, the derived hemispheric and global OH estimates are forced to reconcile the observed trends and gradient for all four compounds simultaneously. However, currently, observations of these gases from the surface networks do not provide more accurate OH abundance estimate than that from MCF.

1. Introduction

The hydroxyl radical (OH) is the primary atmospheric oxidant, and reaction with tropospheric OH is the most important removal process for many ozone-depleting substances (ODSs), their replacements, and other gases that contain one or more hydrogen atoms, for example, hydrochlorofluorocarbons (HCFCs) and hydrofluorocarbons (HFCs). Many of these compounds are also potent greenhouse gases (GHGs) and can exert significant impacts on climate (Rigby et al., 2014; Velders et al., 2015). The rates at which these long-lived gases are removed from the atmosphere, and therefore their lifetimes, are dependent on the atmospheric OH abundance. Their lifetimes are used to calculate future atmospheric abundances based on emission projection scenarios. OH is also responsible for removing methane (CH_4) and many short-lived atmospheric constituents, for example, volatile organic compounds (VOCs) and carbon monoxide (CO). Atmospheric mean OH abundance and its interannual variations are important for understanding the observed long-term atmospheric trends of these trace gases (e.g., McNorton et al., 2016; Rigby et al., 2017; Turner et al., 2017). An accurate estimate of present-day atmospheric OH can lead to an improved understanding of the processes affecting OH and, therefore, better

future projections of air quality, climate, and stratospheric ozone recovery (e.g., Fiore, 2014; Intergovernmental Panel on Climate Change, 2007, 2014; Velders & Daniel, 2014; World Meteorological Organization, 2011, 2014).

Accurate atmospheric measurements of OH abundance are challenging. Hydroxyl radical is produced in the troposphere by the reaction of water vapor with electronically excited atomic oxygen ($O(^1D)$), which is produced by ozone (O_3) photolysis, with a secondary source from the chemical reaction $HO_2 + NO \rightarrow NO_2 + OH$ and analogous reactions (Levy, 1971; Logan et al., 1981). OH production by photodissociation of acetone, peroxides, carbonyls, and nitrous acid is also important in specific regions (Spivakovsky et al., 2000). Tropospheric OH can be measured in situ, but its measurements are difficult due to low atmospheric abundance and a short local lifetime (0.01–1 s) (Stone, Whalley, & Heard, 2012). Most importantly, due to the inhomogeneity in the complex production and loss processes that control OH, which lead to large temporal and spatial variabilities, it is challenging to infer global mean from sparse local measurements (e.g., Fiore, 2014; Montzka et al., 2011).

Atmospheric OH abundance estimates from global chemistry models are also subject to large uncertainties. Recent international multimodel analyses, the Stratosphere-troposphere Processes and their Role in Climate (SPARC) Lifetime Report (SPARC, 2013) and the Atmospheric Chemistry and Climate Model Intercomparison Project (ACCMIP) (Lamarque et al., 2013), illustrate that models show a large spread in simulated global mean OH despite identical anthropogenic emissions of VOCs and NO_x ($NO + NO_2$) used in the models (Naik et al., 2013; Voulgarakis et al., 2013).

IIt was discovered in the late 1970s that tropospheric OH abundance could be inferred using the observed atmospheric rate of change for methyl chloroform (CH_3CCl_3) (MCF) and estimates of its anthropogenic emissions (Lovelock, 1977; Prather et al., 2012; Prinn et al., 1983, 1987; Singh, 1977). MCF works well as a reference gas for deriving atmospheric OH abundance because its sources are relatively well known and its primary sink is OH oxidation. MCF has, since then, been used as the reference gas to infer global OH abundance (e.g., Montzka et al., 2000, 2011; Prinn et al., 2000, 2005; Rigby et al., 2013). MCF was primarily used as an industrial solvent. Its main loss is OH oxidation, with stratospheric photolysis and ocean uptake providing additional minor sinks (12% and 6% of the total loss, respectively) (SPARC, 2013). As an ODS, MCF is controlled under the 1987 Montreal Protocol and its subsequent amendments. Its production and consumption were phased out in developed countries in 1996 and in developing countries in 2015. As a result, atmospheric MCF levels have rapidly declined from peak values of over 100 parts per trillion (ppt) dry mole fraction in the 1990s to about 3.5 ppt by 2014 (Rigby et al., 2017). With a lifetime of about 5 years (SPARC, 2013), MCF atmospheric mixing ratios are expected to drop below 0.5 ppt by 2025. These levels are comparable with measurement repeatability, which will make it difficult to continue to use MCF as a reference indicator for atmospheric OH abundance. Therefore, it is important to find a reliable MCF alternative to infer global mean OH abundance (Huang & Prinn, 2002; Lelieveld et al., 2004, 2006). Under climate change and changing emissions of industrial pollutants, other compounds such as water vapor, O_3, CO, CH_4, and NO_x ($NO + NO_2$) will also change, impacting atmospheric OH. A new

proxy gas or alternative method is needed to provide a means to continue to monitor how atmospheric OH changes as the composition of the atmosphere changes in the future.

In this study, we combine information from surface trace gas observation networks and a multimodel analysis from the SPARC Lifetime Assessment (SPARC, 2013) (section 2) to demonstrate (a) how global trend and interhemispheric mixing ratio differences of long-lived trace gases can be used to derive their global emissions and lifetimes (section 3), (b) what research efforts are needed to reduce the uncertainty in the derived emissions and atmospheric OH abundance estimates in the proposed gradient trend-based method (section 3), and (c) how a combination of multiple OH-removed trace gases with a range of atmospheric lifetimes provide the best constraint on atmospheric OH abundance and its spatial and temporal variability (section 4). A summary is presented in section 5.

2. Global OH Abundance and Trace Gas Lifetimes: Lessons Learned From the SPARC (2013) Model Simulations

For this analysis, we focus on the long-lived trace gases (lifetime >1 year) that are primarily removed by reaction with OH in the troposphere and can impact the stratospheric ozone chemically and/or radiatively: CH_3CCl_3, CH_4, CH_3Cl, and CH_3Br and HCFC-22, HCFC-141b, HCFC-142b, HFC-23, HFC-32, HFC-125, HFC-134a, HFC-143a, and HFC-152a.

2.1. Models and Simulations

Model results from five three-dimensional (3-D) chemistry-climate models (CCMs) and one two-dimensional (2-D) model that participated in SPARC (2013) (see Table S1 in the supporting information for model list) are used in this study. Specifically, we use results from two SPARC (2013) simulations: (1) a transient simulation from 1960 to 2010 (TRANS) driven with time-dependent surface boundary conditions for GHGs (CO_2, CH_4, and N_2O) and ODSs (with specified global uniform surface mixing ratios), sea ice, and sea surface temperatures and (2) a time-slice simulation with year 2000 surface boundary conditions (TS2000) (Chipperfield et al., 2014). All models used kinetic recommendations from Jet Propulsion Laboratory 10–6 (Sander et al., 2011). Model simulation descriptions are included in Text S1 and Table S1 in the supporting information. The six models are divided into two groups according to how tropospheric OH was treated: (i) GEOSCCM (Pawson et al., 2008) and GSFC2D (Fleming et al., 2011) did not include a detailed tropospheric chemistry scheme but prescribed their tropospheric OH with recommended 3-D monthly values from Spivakovsky et al. (2000) and (ii) SOCOL (Revell et al., 2015), ULAQ (Pitari et al., 2014), UMUKCA (Bednarz et al., 2016), and WACCM (Garcia et al., 2007) used fully coupled stratosphere-troposphere chemistry schemes, which calculated interactive OH abundance in the troposphere based on surface emissions of NO_x, CO, and nonmethane hydrocarbons from the Coupled Model Intercomparison Project Representative Concentration Pathways 4.5 scenario (Lamarque et al., 2011). We also include atmospheric OH abundance and trace gas lifetime estimates from a 12-box Bayesian inversion model (IM) (Rigby et al., 2013). The 12-box inversion model participated in SPARC (2013) as well and used the same industrial-based surface emissions for MCF as the global CCMs.

In addition to prescribing monthly varying global uniform surface mixing ratios (mixing ratio boundary conditions or MBCs) for ODSs, the models included two surface emission-based (flux boundary conditions or FBCs) tracers—MCF $(CH_3CCl_3)_{FBC}$ and HCFC-22 $(CHClF_2)_{FBC}$. These two gases were started with the same initial conditions as their MBC parallels, MCF_{MBC} and HCFC-22_{MBC}, in January 1960, and evolved with geographically resolved population-based surface emissions (McCulloch et al., 2001, 2002) and atmospheric losses via reaction with OH, O(1D), Cl, and photolysis. Unlike the MBC ODSs, these FBC gases were not coupled into the full chemistry, which means that Cl released from MCF_{FBC} and HCFC-22_{FBC} are not accounted for in the stratospheric chlorine budget and ozone chemistry.

In this study, we also include GEOSCCM model results from a new simulation for 1960–2010. This updated run has the same model setup as the SPARC (2013) TRANS run but is conducted at a horizontal resolution of 1° × 1°, as compared to the 2° × 2.5° (SPARC 2013) GEOSCCM run. The model outputs were archived at 50 vertical layers with 20 tropospheric layers, in contrast to only seven tropospheric output layers from the SPARC (2013) simulations. The better resolved tropospheric representation is important for accurate model representation and analysis of surface concentration gradients. In addition, the new TRANS run includes surface oceanic loss for MCF_{FBC} (not included in the SPARC (2013) simulations), which leads to a better agreement with surface MCF observations.

For all these models that participated in SPARC (2013), monthly atmospheric losses (unit: moles/moles air/s) of the four primary loss mechanisms, for example, reaction with OH, $O(^1D)$, Cl, and photolysis, at all model grids (from surface to 0.1 hPa) were required as standard output. The atmospheric loss rates for the targeted ODSs, GHGs, and HFCs were used together with their atmospheric burdens to calculate atmospheric lifetimes and partial lifetimes with respect to each loss mechanism. The steady state lifetime (τ_{ss}) for each gas were calculated using the last 10 years' model output from the TS2000 simulation, and the transient lifetime (τ_{trans}) for 2000 were calculated as the model annual mean burden divided by the global atmospheric loss in 2000. The partial lifetimes were determined as the global burden divided by the globally integrated loss via the individual loss mechanism, for example, reaction with OH.

2.2. Correlation Between Global OH and Trace Gas Lifetimes

For our targeted trace gases that are primarily removed by OH oxidation, the tropical middle and lower tropospheric OH abundance plays the key role in determining their lifetimes. Zonally integrated atmospheric loss rates for MCF, CH_4, and HCFC-22 are shown as examples in Figure 1. Reaction with OH accounts for more than 90% of the atmospheric loss for these species. MCF features a secondary loss pathway through lower stratospheric photolysis (10% of the atmospheric sink), and CH_4 has minor loss pathways via reaction with $O(^1D)$ and Cl. About 75–90% of the atmospheric removal of these gases occurs between 60°N and 60°S with more than 50% of the loss in the tropical middle and lower troposphere (30°N–30°S and below 500 hPa). Because these trace gases are lost mainly by their reactions with tropospheric OH, an approximate linear anticorrelation is expected between the model-derived atmospheric lifetimes and global mean mass-weighted

model OH for these species (see Text S2). The expected anticorrelation is confirmed in our multimodel analysis, as demonstrated in Figure 2a.

The multimodel mean MCF steady state atmospheric lifetime is 4.6 ± 0.6 years (1σ variance) for the present-day atmosphere (calculated using model results from the TS2000 simulations). Similar multimodel variances (14–16% of the multimodel mean) are calculated for the other targeted gases (see Table S2). These large variances in modeled lifetimes are due to the differences in modeled OH. We refer to the global mass-weighted tropospheric mean OH concentration as $[OH]_{GM}$, calculated using model OH fields below 200 hPa. The modeled $[OH]_{GM}$ ranges from 1.01 to 1.30 × 10^6 molecules/cm^3 (Figure 2b), with the four CCMs that calculate their own "full chemistry" having $[OH]_{GM}$ between 1.20 and 1.30 × 10^6 molecules/cm^3. While previously reported OH concentrations show significant differences due to model domain and spatial resolution differences (e.g., Lawrence, Jöckel, & von Kuhlmann, 2001), the majority of the published mass-weighted $[OH]_{GM}$ estimates derived from MCF observations range from 0.94 to 1.0 × 10^6 molecules/cm^3 for $[OH]_{GM}$ below 200 hPa (Table 1). The SPARC (2013) models' $[OH]_{GM}$ values are 20–30% higher than the published $[OH]_{GM}$ abundances (Table 1). Model OH abundance estimates from the recent Atmospheric Chemistry and Climate Modeling Intercomparison Project (ACCMIP) multimodel analysis show similarly high $[OH]_{GM}$ with a large variance (mean ± 1σ of 1.11 ± 0.18 × 10^6 molecules/cm^3) (Voulgarakis et al., 2013). The SPARC (2013) intermodel variations in the simulated local OH abundance are larger than those seen in the model $[OH]_{GM}$. The tropical mean vertical profiles (Figure 2b) suggest that all models have higher OH concentrations in the tropical lower troposphere than the Spivakovsky et al. (2000) profile. The modeled OH number density in the tropical lower troposphere, where OH loss plays a critical role in determining the atmospheric lifetime of the targeted gases, differ up to a factor of 2 among individual models. The comparison of the zonal mean cross section of atmospheric OH also shows significant intermodel variability; the modeled OH distributions from SOCOL, ULAQ, and WACCM feature higher OH levels in the Northern Hemisphere (NH) while those in GSFC2D, GEOSCCM, and UMUKCA are relatively symmetric between the NH and the Southern Hemisphere (SH) (Figure 3).

Lifetimes calculated using 3-D chemistry models also differ due to differences in lifetime definitions, for example, τ_{ss} calculated for a system that is at or near steady state versus τ_{trans} that refers to instantaneous lifetime that is not in steady state. Lifetimes can also differ due to variations in simulated atmospheric distributions of the trace gases, for example, uniform surface mixing ratios versus realistic flux-based mixing ratios (Prather & Spivakovsky, 1990). The SPARC (2013) model lifetime differences due to these variations are small compared to intermodel chemical differences associated with differing OH abundances (1σ variance intermodel of 14–16% for τ_{ss}) (see Figure S1b in the supporting information). The mean differences in modeled τ_{ss} from the TS2000 run and τ_{trans} in 2000 from the TRNAS run are within ±1% for MCF, HCFC-22, and CH_4. Despite the fact that MCF_{FBC} and MCF_{MBC} differ significantly in their atmospheric distributions and total burden (Figure S1), their lifetimes differ by <0.2% in the same model simulation. HCFC-22_{FBC} and HCFC-22_{MBC} show similar results (not shown), with a lifetime difference of 0.8%. These

results are comparable to the 1.5% difference reported for HCFC-22 lifetime in Prather and Spivakovsky (1990).

The SPARC (2013) results suggest that the largest uncertainty in the modeled lifetimes of long-lived, OH-removed ODSs and GHGs is tied to the models' ability to accurately calculate OH abundance in global chemistry models, which remains a challenging task (Fiore, 2014).

2.3. Correlation of OH Partial Lifetimes

Despite the large modeled $[OH]_{GM}$ differences, the lifetimes with respect to reaction with OH, τ_{OH}, of other species are well correlated with $\tau_{OH,MCF}$ ($r = 0.991–0.996$) among the SPARC (2013) global models and the 12-box IM (Figure 4). The multimodel regression slope of τ_{OH} for a targeted gas, A, against $\tau_{OH,MCF}$ agrees well with the best fit inverse ratio of their thermal reaction rates with OH, $k_{OH\text{-}MCF}/k_{OH\text{-}A}$, at 272 K. This linear correlation of τ_{OH} between the OH-removed trace gases was suggested previously by Prather and Spivakovsky (1990) and Spivakovsky et al. (2000), but the best fit temperature was revised from the original 277 K in Prather and Spivakovsky (1990) to 272 K in Spivakovsky et al. (2000) to reflect the change in the model OH distribution between the two studies. It is important to point out that the above studies were based on a single model analysis. However, results from this work suggest that this tight correlation between τ_{OH} of long-lived trace gases is robust when multiple models are considered, despite the fact that these global chemistry models all have different $[OH]_{GM}$ and OH distributions. The regression slopes of $\tau_{OH,A}$ versus $\tau_{OH,MCF}$ calculated with the multimodel ensemble results agree well with the $k_{OH\text{-}MCF}/k_{OH\text{-}A}$ ratio at 272 K for all examined species and the correlation holds for all steady state and transient lifetimes for both the MBC and FBC tracers from all models that participated in SPARC (2013).

While this linear correlation of τ_{OH} was suggested first by Spivakovsky et al. (2000) based on their model results, our multimodel-based analysis confirms that it is feasible to derive τ_{OH} of a targeted species, A, by scaling $\tau_{OH,MCF}$ using the ratio of the thermal reaction rates at 272 K,

$$\tau_{OH,A} = \tau_{OH,MCF} \times k_{OH-MCF}(272\ \mathrm{K})/k_{OH-A}(272\ \mathrm{K}) \quad (1)$$

Therefore, it is possible to consider the use of another long-lived compound that is primarily removed by OH in the troposphere, for example, CH_4, CH_3Cl, CH_3Br, HCFCs, or HFCs, as a new reference gas to infer $[OH]_{GM}$ and to derive $\tau_{OH,A}$ for the other long-lived gases, given the growing difficulty associated with using MCF in this analysis.

In summary, here is a list of important findings on atmospheric OH abundance and distribution and the resulted long-lived trace gas lifetimes from the SPARC (2013) multimodel analysis:

1. In spite of the atmospheric removal being dominated by the removal at the tropics and the intermodel differences for [OH] at the tropics being larger than

the intermodel difference of $[OH]_{GM}$, within the same model, the model $\tau_{OH,A}$ for different trace gases is correlated with model $[OH]_{GM}$.

2. Multimodel analysis confirms that $\tau_{OH,A}$ can be derived by scaling τ_{OH} of a reference gas using the ratio of the thermal reaction rates at 272 K, despite the large differences in model OH.

3. For long-lived species (lifetime >1 year) that are well mixed in the troposphere and are primarily removed in the troposphere, the differences between steady state and transient lifetime in the 2000 conditions are small, less than 1%.

4. The difference in lifetimes from the FBC and MBC trace gases is small, less than 1% for HCFC-22 and MCF.

3. Approaches for Deriving Emissions and Trace Gas Lifetimes From Surface Observations

3.1. Deriving Emissions and Lifetimes Using the Global Mean Mixing Ratio Trend

The rate of change of the mean global atmospheric mixing ratio (tendency) of a trace gas, for example, MCF, is a balance of its emissions and losses. For long-lived species (lifetime >1 year) that are well mixed in the troposphere, it is feasible to mathematically link the rate of global mixing ratio change with its global emissions and loss as the following:

$$\frac{\partial C_g}{\partial t} = f \cdot E - \frac{C_g}{\tau} \quad (2)$$

where C_g is the global mean mixing ratio and E represents the global emissions. f is a scaling factor that converts global atmospheric mass (gigagrams or Gg) to mixing ratio (ppt). It is important to note that for short-lived trace gases that feature significant spatial and temporal variations in their tropospheric mixing ratios and losses, this approach is not suitable. Traditionally, the observed MCF global trend from surface monitoring networks has been combined with bottom-up MCF emissions (emissions calculated based on reported industrial production, usage, and release to the atmosphere) to infer its lifetime and, subsequently, $[OH]_{GM}$ (Montzka et al., 2011; Prinn et al., 2000, 2005; Rigby et al., 2013), since $1/\tau_{OH}$ is highly dependent on $[OH]_{GM}$. This emission trend-based method works well for the primarily human-made compound MCF because emissions are well known (McCulloch & Midgley, 2001). Production is known because MCF is a controlled compound under the Montreal Protocol, which requires each party to fully report annual production and consumption, and most of this production is quickly emitted into the atmosphere.

The lack of full global bottom-up emission estimates is the main obstacle in finding a MCF alternative OH reference gas. Acquiring an accurate bottom-up global emission estimate is challenging for compounds that have large natural sources, for example, CH_4, CH_3Cl, and CH_3Br. Hence, the potential MCF alternative is likely to be found among the exclusively human-made HCFCs and HFCs for which (1) their production, sales, and

usage are reported either by the Montreal Protocol parties or United Nations Framework Convention on Climate Change (UNFCCC) and (2) their atmospheric concentrations are monitored continuously. However, while production and consumption of HCFCs and HFCs are available for developed countries from their UNFCCC National Inventory submissions, China, and some other developing countries (Velders et al., 2015), the HCFC and HFC emissions are highly uncertain and the developed country emissions as reported to the UNFCCC account for only about 50% of the total emissions that inferred from the observed abundances (Lunt et al., 2015; Montzka et al., 2015).

Equation (2) can also be used with the observed global trend to derive global emissions if accurate estimates of lifetime are available. An example of this trend lifetime-based emission for MCF is shown in Figure 5 (top plot, gray line).

3.2. Deriving Emissions Using Interhemispheric Mixing Ratio Difference

3.2.1. Method and Examples Using MCF and Other Trace Gases—In this study, we introduce a new approach to infer global emissions for the long-lived trace gases by using their observed mean mixing ratio differences between the NH and the SH. Besides the long-lived ODSs that are primarily removed by OH, for example, CH_4, CH_3Cl, and CH_3Br, there are three abundant HCFCs (HCFC-22, HCFC-141b, and HCFC-142b) (atmospheric mixing ratios >20 ppt) and six abundant HFCs (HFC-23, HFC-32, HFC-125, HFC-134a, HFC-143a, and HFC-152a) (atmospheric mixing ratios >2 ppt), whose atmospheric abundances have been measured continuously in the Advanced Global Atmospheric Gases Experiment (AGAGE) (Prinn et al., 2000) and National Oceanic and Atmospheric Administration–Global Monitoring Division (NOAA-GMD) (Montzka et al., 2015) surface network stations. We will assess these gases in determining which ones, if any, might be good choices for MCF alternatives.

Similar to equation (2), we can express the rate of change of the hemispheric mean mixing ratios of a long-lived trace gas for the NH (C_n) and the SH (C_s) as

$$\frac{\partial C_n}{\partial t} = 2f \cdot E \cdot F_n - \frac{C_n}{\tau_n} - \frac{(C_n - C_s)}{X_{ns}} \tag{3}$$

and

$$\frac{\partial C_s}{\partial t} = 2f \cdot E \cdot (1 - F_n) - \frac{C_s}{\tau_s} - \frac{(C_s - C_n)}{X_{ns}} \tag{4}$$

where F_n is the fraction of global emissions emitted in the NH and X_{ns} is the exchange time between hemispheres. Note that a conversion factor $2f$ is used for the hemispheric values because the total number of air molecules in each hemisphere is exactly half of the global number. Subtracting equation (4) from equation (3) yields

$$\frac{\partial \Delta C_{n-s}}{\partial t} = 2f \cdot E \cdot (2F_n - 1) - (\frac{C_n}{\tau_n} - \frac{C_s}{\tau_s}) - \frac{2\Delta C_{n-s}}{X_{ns}} \tag{5}$$

Together, equations (2) and (5) form a basic set of equations to construct a two-box model, one box for each hemisphere, with which the observed ΔC_{n-s} and global trend of a trace gas can be used to derive its global emissions and lifetime. In the two-box model, the global trend of a trace gas can be expressed as

$$\frac{\partial C_g}{\partial t} = a \cdot \underbrace{\frac{\partial \Delta C_{n-s}}{\partial t}}_{\text{(A)}} + a \cdot \underbrace{(\frac{C_n}{\tau_n} - \frac{C_s}{\tau_s})}_{\text{(B)}} + a \cdot \underbrace{\frac{2\Delta C_{n-s}}{X_{ns}}}_{\text{(C)}} - \underbrace{\frac{C_g}{\tau}}_{\text{(D)}} \tag{6}$$

where $a = 1/(4F_n - 2)$. The four terms on the right of equation (6) are (A) the rate of change of ΔC_{n-s}, (B) the adjusted ΔC_{n-s} due to the different chemical decay in the NH and SH, (C) the adjusted ΔC_{n-s} due to the exchange between hemispheres, and (D) the global chemical decay. Terms A, B, and C appear due to the asymmetry of emission partition between the two hemispheres. The sum of terms A + B + C equals to $f \bullet E$ in equation (2). Therefore, together, these three terms provide quantitative information on global emissions inferred from the observed ΔC_{n-s}. For trace gases with small emissions, for example, MCF in recent years, equation (6) simplifies to equation (2), with which the observed global trend alone can be used to derive atmospheric lifetime.

If we assume that $\tau_n = \tau_s = \tau$ (the implication of a potential OH interhemispheric abundance difference is discussed in section 3.2.2.3), we can rearrange the terms in equation (5), which yields

$$\Delta C_{n-s} = \frac{f}{a \cdot b} \cdot E - \frac{1}{b} \cdot \frac{\partial \Delta C_{n-s}}{\partial t} \tag{7}$$

where $b = 1/\tau + 2/X_{ns}$. For trace gases that have steady emissions or relatively small increases in emissions, which are true for all targeted gases in most years in the past decades, $\partial \Delta C_{n-s}/\partial t/b$ is at least 1 order of magnitude smaller than ΔC_{n-s} for our targeted long-lived trace gases. Therefore, for these gases, ΔC_{n-s} should be approximately a linear function of their global emissions. Model ΔC_{n-s} for MCF_{FBC} and $HCFC\text{-}22_{FBC}$ from the new GEOSCCM TRANS simulation confirms this linear dependence of ΔC_{n-s} on global emissions (Figure 6). As a result of this quasi-linear dependence, the observed ΔC_{n-s} can be used as an empirical proxy to derived global emissions for the long-lived GHGs, ODSs, and HFCs, given reasonable estimates of F_n and X_{ns}.

To demonstrate the validity of our proposed two-box model approach, we assess the gradient-based MCF global emissions with the inventory-based bottom-up estimates

(McCulloch et al., 2001, 2002) and those derived from the global trend and lifetime (Figure 5a). First, we determine the MCF lifetime using the observed global trend from the AGAGE network from 1998 to 2012. During this time period, global emissions were near zero and the MCF trend is predominantly determined by the global chemical decay (D) (Figure 5b, light red shading), which yields a total lifetime of 5.2 years for MCF. Second, we determine X_{ns} using observations from 1992 to 1997. During this period, (C) and (D) are the two dominate contributing terms in the global trend (Figure 5b, blue shading). Together, they explain more than 90% of the global decline rate. With the 5.2 year lifetime estimated from the MCF global trend, we estimate an interhemispheric exchange time (X_{ns}) of ~1.3 years from equation (6). The derived X_{ns} agrees well with the previous estimates of 1.3–1.4 years for long-lived gases (e.g., Geller et al., 1997; Heimann & Keeling, 1986; Liang et al., 2014; Maiss & Levin, 1994). Third, we calculate the global emissions for 1980–2012 (Figure 6a, red line), which equal the sum of terms A, B, and C, divided by the ppt and mass conversion factor f. Note that term B is only ~10% of term C. Thus, the derived global emissions are not very sensitive to variations in the MCF lifetime estimate. The gradient-based emissions (Figure 5a, red line; mean value of 238 Gg/yr between 1980 and 2012) agree very well with top-down global emissions derived using the global MCF trend and a MCF lifetime of 5.2 years (Figure 5a, red line; mean value of 237 Gg/yr between 1980 and 2012). This gives confidence in the robustness of using the observed ΔC_{n-s} to derive emissions. Both observation-based top-down estimates are on average ~17% lower than the inventory-based bottom-up emissions (Figure 5a, black line) during 1980–2012.

Using the 1980 atmospheric concentrations as an initial condition and calculating the atmospheric concentrations with the gradient-based emissions, we find that the optimal MCF lifetime that matches the observed global MCF trend for 1980–2012 is 5.2 years, which matches the value derived with only the 1998–2012 observations. When combined with an ocean lifetime of 94 years and a stratospheric photolysis lifetime of 46 years from SPARC (2013), a total lifetime of 5.2 years yields τ_{OH} of 6.2 years, implying $[OH]_{GM}$ of 1.12×10^6 molecules/cm^3. The lifetime and $[OH]_{GM}$ estimates agree well with results from the previous observation-based calculations (Montzka et al., 2000; Prinn et al., 2000, 2005; Rigby et al., 2017; SPARC, 2013).

The gradient-based emissions (derived with the optimal X_{ns} as discussed in section 3.2.2) also work well for HCFCs and HFCs. When these emissions are compared against the trend lifetime-based emissions (derived using the observed global trends and their best estimate lifetimes scaled from τ_{MCF}), for HFC-32, HFC-134a, HCFC-22, and HFC-152a, the two emission estimates agree well with each other in both the magnitude and year-to-year variations (Figure 7, right). Even during years when abrupt increases and decreases in global emissions occurred, the gradient-based emissions match well with the trend lifetime-based emission estimates, confirming the effectiveness in deriving emissions using the observed gradient. In general, both top-down emission estimates are much higher than the UNFCCC inventory-based bottom-up emissions for all three HFCs, likely due to the incomplete global reporting of emissions (Rigby et al., 2014; Velders et al., 2015).

3.2.2. Uncertainties in the Global Emission Estimate—The accuracy of a derived emission estimate with the gradient trend-based two-box model approach relies heavily on F_n, X_{ns}, and the NH/SH OH abundance ratio estimates for these gases.

3.2.2.1. NH Emission Fraction (F_n): Since the gradient trend-based approach derives emissions using equation (5), F_n is a key element in this approach. For all the long-lived gases of interest to this work, F_n most likely varies between 0.5 (half of the emissions occur in NH and half in SH) and 1.0 (all emissions occur in NH). This is because human activities are the main sources, and with most of the population living in the NH, the majority of emissions are expected to occur in the NH. The derived emissions have the least uncertainty when F_n has values close to 1. As F_n decreases from 1 to 0.5, the uncertainty in the derived emissions grows rapidly with the same small change in F_n. In the idealized case when F_n is 0.5, the observed gradient reflects purely the chemical destruction asymmetry between the two hemispheres and no longer offers any information on emission strength. Since CH_4, CH_3Br, and CH_3Cl all have significant natural sources with emissions that occur in both NH and SH, their F_n values are highly uncertain and have large seasonal and interannual variations, which makes it difficult to derive accurate global emissions using the gradient-based method.

For the human-made compounds that are predominantly produced and emitted in the NH, for example, HCFCs and HFCs, F_n typically varies between 0.9 and 1.0. Inventory-based bottom-up emissions of HCFCs and HFCs can be estimated from the production and usage reported for the Non-Article 5 (developed) countries (thick black lines in Figure 7, right). While these emission estimates are not full global bottom-up emission estimates, it is possible to estimate the approximate F_n for these compounds. For example, annual F_n calculated from these emissions varies from 0.90 to 1.0 for HFC-32, 0.97 to 1.0 for HFC-134a, and 0.99 to 1.0 for HFC-152a during 1990–2012. Although these emission estimates do not include emissions from China and India, they provide an estimate of the minimum F_n as the addition of Chinese and Indian emissions would increase F_n values closer to 1. HCFC-22 is used primarily within refrigeration and air conditioning systems as the working fluid and in the extruded polystyrene foam industries. The HCFC-22 F_n is estimated to be 0.90 for HCFC-22 based on the emission distribution from the Global Emissions Inventory Activity center (http://www.geiacenter.org/), which distributes HCFC-22 emissions among countries using the CFC-12 distribution from 1990, calculated in McCulloch et al. (1994).

The two-box model sensitivity calculation suggests that a ±0.05 change in F_n can lead to ~10–15% change in the gradient-based emissions for the major HCFCs and HFCs. For example, for the 2000–2014 period, a ±0.05 change in F_n changes the derived emissions by ±11% for HFC-32 and HFC-152a, ±12% for HFC-134a, and ±14% for HCFC-22 (light red shadings in Figure 7, right). The percentage change in the long-term trends reflects the relative balance between the total atmospheric burden, the additional mass emitted (emissions) into the atmosphere, and the amount removed from the atmosphere (loss) each year. Therefore, percentage changes in emissions are not directly proportional to changes in long-term trends (hence OH abundance). The 11% emission variation due to the ±0.05 F_n

variation changes the HFC-32 trend by ±13%, while the 14% emission change leads to a ±33% variation in the HCFC-22 trend (Figure 7, left).

3.2.2.2. The North-South Exchange Time Scale (X_{ns}): The two-box model analysis suggests that X_{ns} is a key unknown variable and that an accurate estimate of X_{ns} is essential to improving the accuracy and reducing the uncertainty in the gradient-based emission estimate. Here we show a two-box model sensitivity results for HFC-134a, HFC-32, HFC-152a, and HCFC-22 as examples.

The best estimate lifetimes of these HFCs and HCFC-22 (Table 2) were calculated using the atmospheric OH abundance derived with MCF measurements (Carpenter et al., 2014; SPARC, 2013). Since the uncertainty in the current MCF-derived $[OH]_{GM}$ is relatively small and τ_{OH} of the OH-removed gases can be calculated accurately by scaling $\tau_{OH,MCF}$ (section 2), the uncertainty in these lifetimes is also relatively small. Our two-box model analysis suggests that it is not possible to find a single X_{ns} value that reconciles the observed trends and the current best estimate lifetimes for all four gases simultaneously. With the MCF-derived X_{ns} of 1.3 years, the two-box model underestimates the HFC-32 and HCFC-22 trends but overestimates the HFC-152a trend (Figure 7, left, gray lines). The optimal X_{ns} for matching the observed global trend and best estimate lifetime varies from 1.1 years for HCFC-22 to 1.5 years for HFC-152a (Figure 7, left, dark red lines). The case with HFC-134a appears more complicated. While a constant X_{ns} for the 2000–2012 period works well for HFC-32 and HFC-152a and relatively well for HCFC-22, the best fit X_{ns} changes from 1.8 years for 2000–2005 to 1.1 years for 2006–2014 for HFC-134a (Figure 7, left, dark red lines).

These results imply that, in the parameterized two-box model framework, X_{ns} varies for trace gases that have different lifetimes, as well as for the same gas that has different emission rates of change. The dependence of X_{ns} on lifetimes and emission strength is not surprising. While exchange of the air between the two hemispheres occur in the tropics and the exchange rate is determined by the tropical concentration gradient between the SH and NH tropics, the relative concentration of a compound in the NH tropics versus the NH midlatitude emission region varies with its lifetime and emission strength.

We conducted a suite of model sensitivity simulations using the GSFC2D model to examine the impact of trace gas lifetime and emission strength on X_{ns} and modeled ΔC_{n-s} (Figure 8). We ran four idealized tracers in the GSFC2D model. All four tracers have the same molecular weight as HCFC-22 and are initialized with the same global emissions of HCFC-22 in year 2000 (247,000 t/yr) but were removed with the loss rates (lifetimes) of HCFC-22, HFC-32, HFC-134a, and HFC-152a, respectively. For each tracer, the emissions are increased by either 1%, 5%, 10%, 20%, 40%, or 100%/year and run for 50 years, with the latitudinal emission distribution following that of HCFC-22. These idealized tracers therefore only depend on the lifetime and emission strength. Figure 8a shows how the resulting ΔC_{n-s} is dependent on the lifetime of the tracers, and Figure 8b shows how it is dependent on the rate of emission change. For each sensitivity simulation, the 2-D modeled ΔC_{n-s} increases linearly with increasing emissions, but the regression slope changes as

trace gas lifetime varies from 1.6 years to 14.1 years and the rate of emission change increases from 1%/yr to the extreme 100%/yr. The X_{ns} values for each lifetime and emission scenario can be derived using the modeled emission-gradient regression slope, which equals $f(4F_n - 2)/(1/\tau + 2/X_{ns})$ (see equation (6)). With an emission increase rate of 5%/yr, X_{ns} increases from 1.36–1.37 years for the longer-lived HFC-134a and HCFC-22 to 1.74 years for the relatively short-lived HFC-152a. For an HCFC-22-like tracer, when its emission change rate increases from 1%/yr to the drastic 100%/yr scenario, X_{ns} increases from 1.3 years to 3.3 years. It is important to note that, when year-to-year emission change rapidly, the linear dependence of ΔC_{n-s} on emissions holds and X_{ns} remains constant as long as emissions increase or decrease exponentially, as dictated by equation (7). When rates of emission change vary greatly from year to year, X_{ns} also varies greatly from year to year.

We note that the GSFC2D model provides a good representation of the tropospheric transport processes that are important for the transport and tropical removal of the long-lived species. The model tropospheric age of air derived from simulations using seasonal and latitudinal resolved SF_6 emissions compares well with the age derived from surface SF_6 measurements over the latitude range 90°S–82°N, using the NH midlatitudes (30°N–50°N) as a reference (Waugh et al., 2013). The 1.4 year X_{ns} estimates from the above steady state simulations for the long-lived trace gases agree well with the 3-D CCM simulation results (Liang et al., 2014). However, for our sensitivity simulations, the GSFC2D model tropospheric transport fields are based on a yearly repeating climatology and do not account for interannual variations. In addition to realistic tropospheric transport that is representative of the actual meteorological years, for these HCFCs and HFCs which show abrupt year-to-year change in emissions (Figure 7, right), realistic global emissions of these gases for 2000–2014 are also needed for an accurate estimate of X_{ns}. To derive realistic X_{ns} estimates with 3-D global model calculations that feature both capabilities, extensive computational resources are required to account for the range of trace gas lifetimes and emission scenarios. While such an attempt is not made in this paper, it will be carried out in a follow-up 3-D GEOSCCM analysis.

3.2.2.3. The NH Versus SH OH Abundance Asymmetry: For the above discussion, we assume that the interhemispheric ratio of OH is about 1. Until now, there is no consensus on the interhemispheric ratio of OH abundance. The chemistry-climate models that participated in SPARC (2013), which calculated OH interactively, show higher tropospheric OH levels in the NH than that in the SH (Figure 3). This is similar to the 3-D model simulations from the ACCMIP project, which suggests a multimodel mean $[OH]_{NH}/[OH]_{SH}$ ratio of ~1.4 (Naik et al., 2013). The recent study by Patra et al. (2014), based on an analysis of modeled versus observed MCF ΔC_{n-s} from 2004 to 2011, suggests an $[OH]_{NH}/[OH]_{SH}$ ratio of ~1. This disagreement in the $[OH]_{NH}/[OH]_{SH}$ ratio likely indicates an incomplete understanding of some atmospheric chemical processes that control the OH distribution and/or an inaccurate representation of atmospheric chemistry and transport in current chemistry models, for example, transport across the Intertropical Convergence Zone (Fiore, 2014). Thus, an accurate estimate of the interhemispheric OH ratio is of great significance to improving our understanding of the tropospheric OH, the O_3-HO_x-NO_x chemistry, and their representations in global chemistry models.

Our two-box model sensitivity studies with varying $[OH]_{NH}/[OH]_{SH}$ ratio from 0.9 to 1.1 suggest that this ±0.1 change can lead to a change in the gradient-based global emissions, varying from ~±5% for HFC-32 and HFC-134a to ~±10% for HCFC-22 and HFC-152a (Figure 7, right, light green shading). Hence, an accurate quantification of the $[OH]_{NH}/[OH]_{SH}$ ratio is important to deriving gradient-based emissions.

3.3. Uncertainties in Trace Gas Observations and Kinetic Measurements

3.3.1. Uncertainties in C_g and Interhemispheric Gradient (ΔC_{n-s})—For the AGAGE HFC and HCFC mixing ratio measurements used in this work, the typical repeatability is 0.3% for HCFC-22, 3% for HFC-32, 1% for HFC-143a, and 1.4% for HFC-152a (https://agage.mit.edu/instruments) (e.g., O'Doherty et al., 2014; Prinn et al., 2000). For the observed mixing ratio levels in 2014, the estimated repeatabilities are HCFC-22 ~0.7 ppt (compared to mean NH-SH gradient of ~18 ppt), HFC-32 ~0.3 ppt (compared to mean NH-SH gradient of ~4 ppt), HFC-134a ~0.8 ppt (compared to mean NH-SH gradient of ~10 ppt), and HFC-152a ~0.1 ppt (compared to mean NH-SH gradient of ~5 ppt). Therefore, the observational uncertainties are not major contributors to the emissions or lifetime estimates using gradient trend-based methods, compared to other sources of uncertainty.

However, an important factor that affects the accuracy of the derived OH and lifetimes from the gradient trend-based two-box model approach is related to the representativeness of the surface monitoring network. Specifically, how well does the C_g and ΔC_{n-s} calculated using the AGAGE and NOAA-GMD observations represent the true atmospheric values? Figure 9 shows the probability distribution function (PDF) of the mixing ratio anomalies (with respect to global mean values of that year) in the NH and SH. The hemispheric mean anomalies and ΔC_{n-s} calculated using the GEOSCCM-simulated HCFC-22 at all global surface grid cells ($\Delta C_{n-s,\mathrm{gsurf}}$) versus those calculated using modeled values sampled at the AGAGE and NOAA-GMD stations are also shown. The AGAGE core network contains three NH and two SH sites, with no monitoring stations in the high latitudes. The NOAA network we have considered here consists of 14 surface stations around the globe (10 in the NH, located between 19.5°N and 82.5°N, and 4 in the SH, located between 14.2°S and 90.0°S). As a result of its more representative latitudinal coverage, the NOAA-based mixing ratio PDF is in better agreement with the full global model surface-based PDF than the AGAGE-based PDF. The AGAGE-based PDF is highly biased for NH midlatitude emission regions and the SH low mixing ratio regions due to the absence of high-latitude monitoring sites. Both networks show biases in the PDFs in the tropics, suggesting that the current monitoring stations are too sparse to accurately capture the mixing ratio gradient from the NH high mixing ratio regions to the clean remote SH tropics.

We compare the AGAGE-based and NOAA-based C_g and ΔC_{n-s} with global surface grid-based values, using the 35 year GEOSCCM-simulated HCFC-22 for 1980–2014 from the new TRANS run. The network sampling bias has only a small impact on C_g ($C_{g,\mathrm{AGAGE}}/C_g = 0.986$, $C_{g,\mathrm{NOAA}}/C_g = 0.999$). The impact on ΔC_{n-s} is much larger. NOAA-based ΔC_{n-s} is consistently lower than the global-based ΔC_{n-s} ($\Delta C_{n-s,\mathrm{NOAA}}/\Delta C_{n-s,\mathrm{gsurf}} = 0.89$ with 1 sigma year-to-year variation of 0.02). The AGAGE-based ΔC_{n-s} agrees well with the global

model-based ΔC_{n-s} ($\Delta C_{n-s,\mathrm{AGAGE}}/\Delta C_{n-s,\mathrm{gsurf}} = 0.99 \pm 0.03$), as the low NH mean mixing ratio bias cancels the high SH mean mixing ratio bias. A comparison using the HCFC-22 annual ΔC_{n-s} calculated with the surface observations shows similar results, and the annual mean $\Delta C_{n-s,\mathrm{NOAA}}$ is consistently lower than the annual mean $\Delta C_{n-s,\mathrm{AGAGE}}$ by 6 ± 3% for 2005–2015.

The network sampling bias needs to be carefully considered when the surface network observed ΔC_{n-s} is used in the gradient trend-based approach for OH and lifetime calculation. However, it is important to note that this network sampling bias likely differs for different species. The same calculation for MCF yields $\Delta C_{n-s,\mathrm{NOAA}}/\Delta C_{n-s,\mathrm{gsurf}} = 0.92 \pm 0.03$ and $\Delta C_{n-s,\mathrm{AGAGE}}/\Delta C_{n-s,\mathrm{gsurf}} = 0.95 \pm 0.02$, but the biases remain relatively unchanged during the entire 1980–2015 period while MCF atmospheric mixing ratios go through various phases, a steady increase throughout the 1980s to the 1990s' peak values followed by a sharp decline afterward. The bias difference between HCFC-22 and MCF is likely due to the differences in the emission distribution and/or concentration distribution of these species.

In addition to the differences in ΔC_{n-s} calculated using surface network-based mixing ratios versus full global surface results, ΔC_{n-s} is also different using model results from the free troposphere ($\Delta C_{n-s,\mathrm{trop}}$) versus surface only. The modeled $\Delta C_{n-s,\mathrm{trop}}$, calculated using values from all grid cells below 500 hPa (this pressure level is chosen to avoid complication of the influence of downwelling of aged stratospheric air that has much lower MCF and HCFC-22 mixing ratios), are only 84% of the modeled $\Delta C_{n-s,\mathrm{gsurf}}$ for MCF and 81% of the modeled $\Delta C_{n-s,\mathrm{gsurf}}$ for HCFC-22, respectively. However, it is also important to point out that, if the entire troposphere is considered, X_{ns} is likely shorter than that derived from the surface-based analysis. This is because cross-equator transport of trace gases that are emitted at the NH midlatitude surface to the SH occurs primarily via the upper troposphere (e.g., Bowman & Erukhimova, 2004; Plumb & Mahlman, 1987; Prather et al., 1987). Therefore, the time required for propagation of the surface NH air mass composition signal to the SH surface is longer than the propagation time from the NH free troposphere to the SH free troposphere. These differences in surface-based versus troposphere-based ΔC_{n-s} and X_{ns} suggest that, while it is desirable to include all available surface and aircraft measurements for mass balance calculation, care needs to be taken in how these measurements are integrated in the two-box model parameterized representation.

3.3.2. OH Rate Coefficients—The k-OH rate coefficients have 1 sigma uncertainty factors, $f(272\mathrm{K})$, varying between 1.07 and 1.14 for the four selected potential reference gases (Table 3), compared to 1.14 for MCF (SPARC, 2013). This level of uncertainty impacts the accuracy of the trace gas-based OH and lifetime estimates, but different trace gases show different sensitivities to variations in the k-OH rates uncertainty depending on their atmospheric abundances and emission strengths. A 10% uncertainty in the k-OH rate coefficients changes the two-box model calculated trends, and subsequently, the trend implied $[\mathrm{OH}]_{\mathrm{GM}}$, by 4–8% for the three HFCs (4% for HFC-32, 6% for HFC-134a, and 8% for HFC-152a) and as much as 16% for HCFC-22. Reducing the k-OH rate uncertainties, in particular, the k-OH rate uncertainty for HCFC-22, is important in reducing the uncertainties in the estimates of atmospheric OH and lifetime of the OH-removed trace gases.

4. Multispecies Approach for Deriving $[OH]_{GM}$ and Interhemispheric Differences in OH

Using surface observations from the AGAGE network, we assess the relative contributions of the four identified factors (terms A–D in equation (6)) to the observed global trends for the nine most abundant HCFCs and HFCs during 2005–2014 and compare these results to those derived for MCF (Table 2). During the last two decades, MCF offered a unique opportunity to observe the decay of a trace gas in the atmosphere predominantly due to OH oxidation, as suggested by Spivakovsky et al. (2000) and Montzka et al. (2000). The observed MCF trend during 1998–2014 features a large global chemical decay (term D) and small emission terms A–C. Although human-made HCFCs and HFCs are our best candidates as MCF alternative OH reference gases, none of the nine gases are as good as MCF in the years between 1998 and 2014. Due to their large ongoing emissions, in the gradient trend-based two-box model approach, the magnitude of term C is comparable to or larger than the absolute magnitude of the global decay term (D) for the nine HCFCs and HFCs.

Here we propose that, instead of a single gas, the combination of four trace gases, HFC-32, HFC-134a, HFC-152a, and HCFC-22, in the gradient trend-based framework could improve the accuracy of the derived τ_{OH} and $[OH]_{GM}$. The key basis for this multispecies approach is that their OH lifetimes can be accurately estimated by scaling the thermal reaction rates of a reference gas at 272 K on global and hemispheric scales (see equation (1)). Thus, the derived hemispheric and global OH estimates have to reconcile the observed trends and ΔC_{n-s} for all four compounds simultaneously. This greatly enhances the robustness of the derived results. While the use of HFC-32 and HFC-134a are adequate to obtain reasonable $[OH]_{GM}$ estimates, the addition of HCFC-22 and HFC-152a provides information on the $[OH]_{NH}/[OH]_{SH}$ ratio, which improves the accuracy of the global OH abundance estimate. Iteration of the HFC-32- and HFC-134a-based global OH estimates and the HCFC-22- and HFC-152a-based hemispheric OH estimates need to be performed to find the best τ_{OH} and $[OH]_{NH}/[OH]_{SH}$ ratio that reconciles the observations of all four trace gases. The use of HCFC-22 and HFC-152a also provides information on interhemispheric and seasonal variations of the atmospheric OH abundance. Compared to most of the HCFCs and HFCs in Table 2, these four gases are removed from the atmosphere more predominantly through reaction with OH (>98.5% of the total loss; Table 2), making them better choices as OH reference gases from a chemical loss perspective.

4.1. HFC-32 and HFC-134a for Estimating $[OH]_{GM}$

HFC-32 and HFC-134a are identified among the nine gases as the two best MCF alternatives to infer $[OH]_{GM}$ for the following four reasons: (1) a large global chemical decay term with respect to the annual growth rate (which rules out HFC-23 and HFC-143a), (2) low sensitivity to the $[OH]_{NH}/[OH]_{SH}$ ratio (which rules out HCFC-22 and HFC-152a), (3) predominant loss of OH oxidation (>99%) and small sensitivity of their global loss rates to the kinetic uncertainty in the OH reaction rate coefficient (the 10–14% uncertainty of k(272 K) for HFC-32 and HFC-134a (Table 3) leads to a 4–5% uncertainty in the

derived OH lifetime), and (4) availability of emission history and F_n estimates (which rules out HCFC-141b and HCFC-142b). HFC-32 has advantages over HFC-134a from a bottom-up perspective. Unlike HFC-134a that is mainly used in mobile air conditioning with replacements already available and used, HFC-32 has a continuing use as a component of blends with other HFCs in refrigeration and stationary air conditioning. Emissions and their uncertainties from these systems are reported in the UNFCCC database. On the other hand, many recent aircraft campaigns throughout the NH provide atmospheric measurements of HFC-134a since 2001, but not HFC-32 (Prof. Elliot Atlas, U. Miami, personal communication). These measurements could be used to derive regional emissions for improved F_n estimate, which makes HFC-134a more appealing from a top-down perspective.

4.2. HCFC-22 and HFC-152a for Estimating OH Interhemispheric and Seasonal Variations

When combined with HFC-32 and HFC-134a, HCFC-22 and HFC-152a can provide important information on the potential hemispheric asymmetry in OH abundance. Our OH sensitivity studies using the two-box model suggest that the calculated HCFC-22 and HFC-152a trends are highly sensitive to the potential OH difference between the two hemispheres. The ratios of term B with respect to total growth rates are 0.4 and 7.5 for HCFC-22 and HFC-152a, respectively. Changing the $[OH]_{NH}/[OH]_{SH}$ ratio by ±0.1 can change the HCFC-22 and HFC-152a growth rates by 20% and 12%, respectively. On one hand, the significant contribution from term B implies that these two compounds alone are not good choices as global OH reference gases because the derived emissions and lifetimes are subject to large uncertainties due to the potential OH abundance difference between the hemispheres, for example, $\tau_n \neq \tau_s$ (see Figure 7). On the other hand, this suggests that, with accurate estimates of F_n, X_{ns}, and total lifetime scaled from HFC-32 and HFC-134a, HCFC-22 and HFC-152a observations contain quantitative information that can be used to infer whether there is an asymmetry in the hemispheric OH abundance. HFC-152a also provides information on the seasonal variation of atmospheric OH in the NH and SH. Due to its shorter lifetime of 1.6 years, the observed hemispheric mean of HFC-152a displays significant seasonal variations (with amplitudes of 2 ppt in the NH and 0.5 ppt in the SH, with respect to a global mean mixing ratio of ~7 ppt), in contrast to the longer-lived tracers, for example, HFC-32 (lifetime of 5.4 years), which display much smaller seasonal cycle. Since HFC-152a is mainly used as an aerosol propellant and in open-cell foam blowing, we do not expect its usage and emissions to have a strong seasonal cycle. This observed seasonality mainly reflects the seasonality in its chemical loss, thus providing information on the OH seasonal variation.

5. Summary

Methyl chloroform (MCF) is commonly used as a reference gas for deriving global OH abundance. As a result of the Montreal Protocol regulation, MCF atmospheric mixing ratio has declined rapidly in recent years. Therefore, it is important to find a MCF alternative approach to accurately infer the atmospheric OH abundance. In this study, we utilize observations from surface networks and a multimodel analysis to identify reference gas(es) suitable as MCF alternatives.

While an accurate model representation of atmospheric OH remains a challenge, global chemistry-climate models provide useful information that aids in the search for the next OH proxy gas(es). Model results from the SPARC (2013) simulations suggest that the partial lifetimes with respect to reaction with OH, τ_{OH}, for the long-lived GHGs and ODSs that are primarily removed through tropospheric OH oxidation, are tightly correlated with each other, independent of differences in OH abundance among individual models. The multimodel regression slope of τ_{OH} of a targeted gas, A, against τ_{OH} of a reference gas, τ_{OH}, MCF, in this work, agrees well with the best fit inverse ratio of their OH reaction rates, $k_{OH\text{-}MCF}/k_{OH\text{-}A}$, evaluated at 272 K. This linear correlation of τ_{OH} among the long-lived gases provides two important constraints for deriving global OH and lifetime estimates: (1) the multimodel analysis confirms the Spivakovsky et al. (2000) findings that it is possible to derive τ_{OH} of a target gas by scaling to τ_{OH} of a reference gas and (2) the atmospheric measurements of multiple gases can be combined to reduce the uncertainties of observation-based atmospheric OH abundance and lifetimes of trace gases.

Our analysis shows that a combination of HFC-32, HFC-134a, HFC-152a, and HCFC-22 in a gradient trend-based two-box model approach, with one box for each hemisphere, can be used to estimate atmospheric OH abundance and the likely OH difference between the two hemispheres. The combination of multiple reference gases greatly reduces the uncertainty of the derived global OH abundance and offers additional details on the spatial and temporal variations of OH than the traditional single reference gas approach. The combination of HFC-32 and HFC-134a is suggested as the best MCF alternative to infer global OH abundance and the addition of HCFC-22 and HFC-152a provides valuable information on the interhemispheric ratio and the seasonal variation of tropospheric OH abundance. Our analysis using the gradient trend-based two-box model approach for MCF yields a MCF lifetime of 5.2 years and a global average $[OH]_{GM}$ of 1.12×10^6 molecules/cm^3, agreeing well with previous observation-based estimates that used bottom-up emission inventories for MCF. The approach taken here does not require detailed knowledge of emissions of the four species. The Northern Hemisphere (NH) versus Southern Hemisphere (SH) mixing ratio differences work well as an empirical proxy to derive global emissions and the gradient-based emissions agree well with the trend lifetime-based emissions for all four gases.

As a result of the lack of a global inventory-based emission record and distribution for these reference gases, the gradient trend-based approach is the current best approach to infer atmospheric OH abundance. However, this approach requires realistic estimates of the NH versus SH emission partitions, F_n (can be approximated using the current bottom-up inventory-based emissions), and the NH and SH exchange time, X_{ns}. X_{ns} estimates are complex as X_{ns} varies with trace gas lifetime and emission strength. But accurate X_{ns} estimates can be achieved by conducting extensive 3-D global chemistry model simulations of HFCs and HCFCs with varying lifetimes and emissions. Such an approach is computationally expensive and requires extensive time for designing the experiment and conducting model simulations and will be carried out in a follow-up 3-D GEOSCCM analysis that features realistic atmospheric transport and chemical simulations of HFCs and HCFCs.

Supplementary Material

Refer to Web version on PubMed Central for supplementary material.

Acknowledgments

The NASA Goddard team thanks the NASA Headquarters Atmospheric Composition Modeling and Analysis program for the support of the GSFC2D model and the NNX11AN71G and NNX17AG33G projects. The University of Leeds was supported by the NERC MAPLE project (NE/J008621/1). The SOCOL modeling work was supported by the SNF projects FuMES and SPARC International Project office as well as the CCES project MAIOLICA-2. The work of SCH was supported by the Joint BEIS/Defra Met Office Hadley Centre Climate Programme (GA01101). The UMUKCA team acknowledges use of the MONSooN system, a collaborative facility supplied under the Joint Weather and Climate Research Programme, which is a strategic partnership between the UK Met Office and the Natural Environment Research Council. Olaf Morgenstern has been supported by NIWA as part of its government-funded core research. The National Center for Atmospheric Research (NCAR) is sponsored by the U.S. National Science Foundation. The operation of the AGAGE stations was supported by the National Aeronautics and Space Administration (NASA, USA) (grants NAG5-12669, NNX07AE89G, NNX11AF17G, and NNX16AC98G to MIT; grants NAG5-4023, NNX07AE87G, NNX07AF09G, NNX11AF15G, and NNX11AF16G to SIO); the Department of the Energy and Climate Change (DECC, UK) (contract GA0201 to the University of Bristol); and the National Oceanic and Atmospheric Administration (NOAA, USA) (contract RA133R09CN0062 in addition to the operations of American Samoa station), by the Commonwealth Scientific and Industrial Research Organization (CSIRO, Australia), the Bureau of Meteorology (Australia) and Refrigerant Reclaim Australia, Refrigerant Reclaim Australia, and the Department of Environment and Energy. Matt Rigby was supported by NERC Advanced Fellowship NE/I021365/1. Measurements at NOAA are supported in part by NOAA's Climate Program Office's AC4 program. The AGAGE measurements can be accessed at https://agage.mit.edu, and the NOAA-GMD measurements can be accessed at https://www.esrl.noaa.gov/gmd/hats/. All model data presented in this paper are available from the corresponding author upon direct request.

References

Bednarz EM, Maycock AC, Abraham NL, Braesicke P, Dessens O, & Pyle JA (2016). Future Arctic ozone recovery: The importance of chemistry and dynamics. Atmospheric Chemistry and Physics, 16(18), 12,159–12,176. 10.5194/acp-16-12159-2016

Bousquet P, Hauglustaine DA, Peylin P, Carouge C, & Ciais P. (2005). Two decades of OH variability as inferred by an inversion of atmospheric transport and chemistry of methyl chloroform. Atmospheric Chemistry and Physics, 5(10), 2635–2656. 10.5194/acp-5-2635-2005

Bowman KP, & Erukhimova T. (2004). Comparison of global-scale Lagrangian transport properties of the NCEP reanalysis and CCM3. Journal of Climate, 17(5), 1135–1146. 10.1175/1520-0442(2004)017,1135:COGLTP.2.0.CO;2

Carpenter LJ, Reimann S, Burkholder JB, Clerbaux C, Hall BD, … Yvon-Lewis SA (2014). Ozone-depleting substances (ODSs) and other gases of interest to the Montreal Protocol, In Scientific assessment of ozone depletion: 2014, (Chapter 1, pp. 1.1–1.101). Global Ozone Research and Monitoring Project–Report No. 55, Geneva, Switzerland: World Meteorological Organization.

Chipperfield MP, Liang Q, Strahan SE, Morgenstern O, Dhomse SS, Abraham NL, … Tummon F. (2014). Multi-model estimates of atmospheric lifetimes of long-lived ozone-depleting-substances: Present and future. Journal of Geophysical Research: Atmospheres, 119, 2555–2573. 10.1029/2013JD021097

Crutzen P, & Zimmermann PH (1991). The changing photochemistry of the troposphere. Tellus, 43(4), 136–151. 10.3402/tellusb.v43i4.15403

Fiore AM (2014). Atmospheric chemistry: No equatorial divide for a cleaning radical. Nature, 513(7517), 176–178. 10.1038/513176a [PubMed: 25209794]

Fleming EL, Jackman CH, Stolarski RS, & Douglass AR (2011). A model study of the impact of source gas changes on the stratosphere for 1850–2100. Atmospheric Chemistry and Physics, 11(16), 8515–8541. 10.5194/acp-11-8515-2011

Garcia RR, Marsh D, Kinnison DE, Boville B, & Sassi F. (2007). Simulations of secular trends in the middle atmosphere, 1950–2003. Journal of Geophysical Research, 112, D09301. 10.1029/2006JD007485

Geller LS, Elkins JW, Lobert JM, Clarke AD, Hurst DF, Butler JH, & Myers RC (1997). Tropospheric SF6: Observed latitudinal distribution and trends, derived emissions, and interhemispheric exchange time. Geophysical Research Letters, 24(6), 675–678. 10.1029/97GL00523

Heimann M, & Keeling CD (1986). Meridional eddy diffusion model of the transport of atmospheric carbon dioxide: 1. Seasonal carbon cycle over the tropical Pacific Ocean. Journal of Geophysical Research, 91(D7), 7765–7781. 10.1029/JD091iD07p07765

Huang J, & Prinn RG (2002). Critical evaluation of emissions for potential new OH titrating gases, Journal of Geophysical Research, 107(D24), 4784. 10.1029/2002JD002394

Intergovernmental Panel on Climate Change (2007). In Solomon S, et al. (Eds.), Climate change 2007: The physical science basis. Contribution of Working Group I to the Fourth Assessment Report of the Intergovernmental Panel on Climate Change. Cambridge, United Kingdom and New York, NY: Cambridge University Press.

Intergovernmental Panel on Climate Change (2014). In Core Writing Team, Pachauri RK, & Meyer LA (Eds.), Climate change 2014: Synthesis report. Contribution of Working Groups I, II and III to the Fifth Assessment Report of the Intergovernmental Panel on Climate Change (p. 151). Geneva, Switzerland: IPCC.

Krol MC, Lelieveld J, Oram DE, Sturrock GA, Penkett SA, Brenninkmeijer CAM, … Scheeren HA (2003). Continuing emissions of methyl chloroform from Europe. Nature, 421(6919), 131–135. 10.1038/nature01311 [PubMed: 12520294]

Lamarque JF, Shindell DT, Josse B, Young PJ, Cionni I, Eyring V, … Zeng G. (2013). The Atmospheric Chemistry and Climate Model Intercomparison Project (ACCMIP): Overview and description of models, simulations and climate diagnostics, Geoscientific Model Development, 6(1), 179–206. 10.5194/gmd-6-179-2013

Lamarque L, Kyle GP, Meinshausen M, Riahi K, Smith SJ, van Vuuren DP, … Vitt F. (2011). Global and regional evolution of short-lived radiatively-active gases and aerosols in the Representative Concentration Pathways. De Change, 109(1–2), 191–212. 10.1007/s10584-011-0155-0

Lawrence MG, Jöckel P, & von Kuhlmann R. (2001). What does global mean OH concentration tell us. Atmospheric Chemistry and Physics, 1(1), 37–49. 10.5194/acp-1-37-2001

Lelieveld J, Brenninkmeijer CAM, Joeckel P, Isaksen ISA, Krol MC, Mak JE, … Tans PP (2006). New directions: Watching over tropospheric hydroxyl. Atmospheric Environment, 40(29), 5741–5743. 10.1016/j.atmosenv.2006.04.008

Lelieveld J, Dentener FJ, Peters W, & Krol MC (2004). On the role of hydroxyl radicals in the self-cleansing capacity of the troposphere. Atmospheric Chemistry and Physics, 4, 2337–2344.

Levy H. (1971). Normal atmosphere: Large radical and formaldehyde concentrations predicted. Science, 173(3992), 141–143. 10.1126/science.173.3992.141 [PubMed: 17739642]

Liang Q, Newman PA, Daniel JS, Reimann S, Hall BD, Dutton G, & Kuijpers LJM (2014). Constraining the carbon tetrachloride (CCl4) budget using its global trend and inter-hemispheric gradient. Geophysical Research Letters, 41, 5307–5315. 10.1002/2014GL060754

Logan JA, Prather MJ, Wofsy SC, & McElroy MB (1981). Tropospheric chemistry: A global perspective. Journal of Geophysical Research, 86(C8), 7210–7254. 10.1029/JC086iC08p07210

Lovelock JE (1977). Methyl chloroform in the troposphere as an indicator of OH radical abundance. Nature, 267(5606), 32. 10.1038/267032a0

Lunt MF, Rigby M, Ganesan AL, Manning AJ, Prinn RG, ODoherty S, … Simmonds PG (2015). Reconciling reported and unreported HFC emissions with atmospheric observations. Proceedings of the National Academy of Sciences, 112(19), 5927–5931. 10.1073/pnas.1420247112

Maiss M, & Levin I. (1994). Global increase of SF6 observed in the atmosphere. Geophysical Research Letters, 21(7), 569–572. 10.1029/94GL00179

McCulloch A, Ashford P, & Midgley PM (2001). Historic emissions of fluorotrichloromethane (CFC-11) based on a market survey. Atmospheric Environment, 35(26), 4387–4397. 10.1016/S1352-2310(01)00249-7

McCulloch A, & Midgley PM (2001). The history of methyl chloroform emissions: 1951–2000. Atmospheric Environment, 35.31(2001), 5311–5319. 10.1016/S1352-2310(01)00306-5

McCulloch A, Midgley PM, & Ashford P. (2002). Releases of refridgerant gases (CFC-12, HCFC-22, and HFC-134a) to the atmosphere. Atmospheric Environment, 37(7), 889–902.

McCulloch A, Midgley PM, & Fisher DA (1994). Distribution of emissions of chlorofluorocarbons (CFCs) 11, 12, 113, 114 and 115 among reporting and non-reporting countries in 1986. Atmospheric Environment, 28(16), 2567–2582. 10.1016/1352-2310(94)90431-6

McNorton J, Chipperfield MP, Gloor M, Wilson C, Feng W, Hayman GD, … Montzka SA (2016). Role of OH variability in the stalling of the global atmospheric CH4 growth rate from 1999 to 2006. Atmospheric Chemistry and Physics, 16(12), 7943–7956. 10.5194/acp-16-7943-2016

Montzka SA, Krol M, Dlugokencky E, Hall B, Jöckel P, & Lelieveld J. (2011). Small interannual variability of global atmospheric hydroxyl. Science, 331(6013), 67–69. 10.1126/science.1197640 [PubMed: 21212353]

Montzka SA, McFarland M, Andersen SO, Miller BR, Fahey DW, Hall BD, … Elkins JW (2015). Recent trends in global emissions of hydrochlorofluorocarbons and hydrofluorocarbons: Reflecting on the 2007 adjustments to the Montreal Protocol. The Journal of Physical Chemistry. A, 119(19), 4439–4449. 10.1021/jp5097376 [PubMed: 25405363]

Montzka SA, Spavakovsky CM, Butler JH, Elkins JW, Lock LT, & Mondeel DJ (2000). New observational constraints for atmospheric hydroxyl on global and hemispheric scales. Science, 288(5465), 500–503. 10.1126/science.288.5465.500 [PubMed: 10775106]

Naik V, Voulgarakis A, Fiore AM, Horowitz LW, Lamarque J-F, Lin M, … Zeng G. (2013). Preindustrial to present-day changes in tropospheric hydroxyl radical and methane lifetime from the Atmospheric Chemistry and Climate Model Intercomparison Project (ACCMIP). Atmospheric Chemistry and Physics, 13(10), 5277–5298. 10.5194/acp-13-5277-2013

O'Doherty S, Rigby M, Mühle J, Ivy DJ, Miller BR, Young D, … Fraser PJ (2014). Global emissions of HFC-143a (CH3CF3) and HFC-32 (CH2F2) from in situ and air archive atmospheric observations. Atmospheric Chemistry and Physics, 14(17), 9249–9258. 10.5194/acp-14-9249-2014

Patra PK, Krol MC, Montzka SA, Arnold T, Atlas EL, Lintner BR, … Young D. (2014). Observational evidence for interhemispheric hydroxyl-radical parity. Nature, 513(7517), 219–223. 10.1038/nature13721 [PubMed: 25209800]

Pawson S, Stolarski RS, Douglass AR, Newman PA, Nielsen JE, Frith SM, & Gupta ML (2008). Goddard Earth Observing System Chemistry-Climate Model simulations of stratospheric ozone-temperature coupling between 1950 and 2005. Journal of Geophysical Research, 113, D12103. 10.1029/2007JD009511

Pitari G, Aquila V, Kravitz B, Robock A, Watanabe S, Cionni I, … Tilmes S. (2014). Stratospheric ozone response to sulfate geoengineering: Results from the Geoengineering Model Intercomparison Project (GeoMIP). Journal of Geophysical Research, 119, 2629–2653. 10.1002/2013JD020566

Plumb R, & Mahlman J. (1987). The zonally averaged transport characteristics of the GFDL general circulation/transport model. Journal of the Atmospheric Sciences, 44(2), 298–327. 10.1175/1520-0469(1987)044,0298:TZATCO.2.0.CO;2

Poisson N, Kanakidou M, & Crutzen PJ (2000). Impact of nonmethane hydrocarbons on tropospheric chemistry and the oxidizing power of the global troposphere: 3-dimensional modeling results. Journal of Atmospheric Chemistry, 36(2), 157–230. 10.1023/A:1006300616544

Prather M, McElroy M, Wofsy S, Russell G, & Rind D. (1987). Chemistry of the global troposphere: Fluorocarbons as tracers of air motion. Journal of Geophysical Research, 92(D6), 6579–6613. 10.1029/JD092iD06p06579

Prather M, & Spivakovsky CM (1990). Tropospheric OH and the lifetimes of hydrochlorofluorocarbons. Journal of Geophysical Research, 95(D11), 18,723–18,729. 10.1029/JD095iD11p18723

Prather MJ, Holmes CD, & Hsu J. (2012). Reactive greenhouse gas scenarios: Systematic exploration of uncertainties and the role of atmospheric chemistry. Geophysical Research Letters, 39, L09803. 10.1029/2012GL051440

Prinn RG, Cunnold DM, Rasmussen R, Simmonds PG, Alyea FN, Crawford A, … Rosen R. (1987). Atmospheric trends in methylchloroform and the global average for the hydroxyl radical. Science, 238(4829), 945–950. 10.1126/science.238.4829.945 [PubMed: 17829360]

Prinn RG, Huang J, Weiss RF, Cunnold DM, Fraser PJ, Simmonds PG, … Krummel PB (2005). Evidence for variability of atmospheric hydroxyl radicals over the past quarter century. Geophysical Research Letters, 32, L07809. 10.1029/2004GL022228

Prinn RG, Huang J, Weiss RF, Cunnold DM, Fraser PJ, Simmonds PG, … Miller BR (2001). Evidence for substantial variations of atmospheric hydroxyl radicals in the past two decades. Science, 292(5523), 1882–1888. 10.1126/science.1058673 [PubMed: 11337586]

Prinn RG, Rasmussen RA, Simmonds PG, Alyea FN, Cunnold DM, Lane BC, … Crawford AJ (1983). The Atmospheric Lifetime Experiment, 5: Results for CH_3CCl_3 based on three years of data. Journal of Geophysical Research, 88(C13), 8415–8426. 10.1029/JC088iC13p08415

Prinn RG, Weiss R, Fraser P, Simmonds PG, Cunnold D, Alyea FN, … McCulloch A. (2000). A history of chemically and radiatively important gases in air deduced from ALE/GAGE/AGAGE. Journal of Geophysical Research, 105(D14), 17751–17792. 10.1029/2000JD900141

Prinn RG, Weiss RF, Miller BR, Huang J, Alya FN, Cunnold DM, … Simmonds PG (1995). Atmospheric trends and lifetime of CH_3CCl_3 and global OH concentrations. Science, 269(5221), 187–192. 10.1126/science.269.5221.187 [PubMed: 17789846]

Revell LE, Tummon F, Stenke A, Sukhodolov T, Coulon A, Rozanov E, … Peter T. (2015). Drivers of the tropospheric ozone budget throughout the 21st century under the medium-high climate scenario RCP 6.0. Atmospheric Chemistry and Physics, 15(10), 5887–5902. 10.5194/acp-15-5887-2015

Rigby M, Montzka SA, Prinn RG, White JWC, Young D, O'Doherty S, … Park S. (2017). Role of atmospheric oxidation in recent methane growth. Proceedings of the National Academy of Sciences of the United States of America, 114(21), 5373–5377. 10.1073/pnas.1616426114 [PubMed: 28416657]

Rigby M, Prinn RG, O'Doherty S, Miller BR, Ivy D, Muhle J, … Simmonds PG (2014). Recent and future trends in synthetic greenhouse gas radiative forcing. Geophysical Research Letters, 41, 2623–2630. 10.1002/2013GL059099

Rigby M, Prinn RG, O'Doherty S, Montzka SA, McCulloch A, Harth CM, … Fraser PJ (2013). Re-evaluation of the lifetimes of the major CFCs and CH_3CCl_3 using atmospheric trends. Atmospheric Chemistry and Physics, 13(5), 2691–2702. 10.5194/acp-132691-2013

Sander SP, Abbatt J, Barker JR, Burkholder JB, Friedl RR, Golden DM, … Wine PH (2011). Chemical kinetics and photochemical data for use in atmospheric studies, Evaluation No. 17, JPL Publication 10–6, Pasadena, CA: Jet Propulsion Laboratory. Retrieved from: http://jpldataeval.jpl.nasa.gov

Singh HB (1977). Preliminary estimation of average tropospheric HO concentrations in the northern and southern hemispheres. Geophysical Research Letters, 4(10), 453–456. 10.1029/GL004i010p00453

SPARC (2013). In Ko M, et al. (Eds.), SPARC report on the lifetimes of stratospheric ozone-depleting substances, their replacements, and related species, SPARC Report No. 6, WCRP-15/2013. Zurich, Switzerland. Stratosphere-troposphere Processes And their Role in Climate.

Spivakovsky CM, Logan JA, Montzka SA, Balkanski YJ, Foreman-Fowler M, Jones DBJ, … McElroy MB (2000). Three-dimensional climatological distribution of tropospheric OH: Update and evaluation. Journal of Geophysical Research, 105(D7), 8931–8980. 10.1029/1999JD901006

Spivakovsky CM, Yevich R, Logan JA, Wofsy SC, McElroy MB, & Prather MJ (1990). Tropospheric OH in a three-dimensional chemical tracer model: An assessment based on observations of CH3CCl3. Journal of Geophysical Research, 95, 18,441–18,471. 10.1029/90JD01299

Stone D, Whalley LK, & Heard DE (2012). Tropospheric OH and HO_2 radicals: Field measurements and model comparisons. Chemical Society Reviews, 41(19), 6348–6404. 10.1039/c2cs35140d [PubMed: 22907645]

Turner AJ, Frankenberg C, Wennberg PO, & Jacob DJ (2017). Ambiguity in the causes for decadal trends in atmospheric methane and hydroxyl. Proceedings of the National Academy of Sciences of the United States of America, 114(21), 5367–5372. 10.1073/pnas.1616020114 [PubMed: 28416668]

Velders GJM, & Daniel JS (2014). Uncertainty analysis of projections of ozone-depleting substances: Mixing ratios, EESC, ODPs, and GWPs. Atmospheric Chemistry and Physics, 14(6), 2757–2776. 10.5194/acp-14-2757-2014

Velders GJM, Fahey DW, Daniel JS, Andersen SO, & McFarland M. (2015). Future atmospheric abundances and climate forcings from scenarios of global and regional hydrofluorocarbon (HFC) emissions. Atmospheric Environment, 123, 200–209. 10.1016/j.atmosenv.2015.10.071

Voulgarakis A, Naik V, Lamarque J-F, Shindell DT, Young PJ, Prather MJ, … Zeng G. (2013). Analysis of present day and future OH and methane lifetime in the ACCMIP simulations. Atmospheric Chemistry and Physics, 13(5), 2563–2587. 10.5194/acp-13-2563-2013

Wang JS, McElroy MB, Logan JA, Palmer PI, Chameides WL, Wang Y, & Megretskaia IA (2008). A quantitative assessment of uncertainties affecting estimates of global mean OH derived from methyl chloroform observations. Journal of Geophysical Research, 113, D12302. 10.1029/2007JD008496

Wang Y, Logan JA, & Jacob DJ (1998). Global simulation of tropospheric O_3-NO_x-hydrocarbon chemistry, 2. Model evaluation and global ozone budget. Journal of Geophysical Research, 103(D9), 10,727–10,755. 10.1029/98JD00157

Waugh DW, Crotwell AM, Dlugokencky EJ, Dutton GS, Elkins JW, Hall BD, … Sweeney C. (2013). Tropospheric SF_6: Age of air from the Northern Hemisphere midlatitude surface. Journal of Geophysical Research, 118, 11,429–11,441. 10.1002/jgrd.50848

World Meteorological Organization (2011). Scientific assessment of ozone depletion: 2010, Global Ozone Research and Monitoring Project— Report No. 52, pp. 516, Geneva, Switzerland.

World Meteorological Organization (2014). Scientific assessment of ozone depletion: 2014, World Meteorological Organization, Global Ozone Research and Monitoring Project—Report No. 55, pp. 416, Geneva, Switzerland.

Key Points:

- The interhemispheric mixing ratio difference of a long-lived gas can be used as a quantitative proxy to derive global emissions
- The combination of multiple species in the gradient trend-based approach should reduce the uncertainties in global OH abundance estimate
- HFC-32 and HFC-134a, with the help of HFC-152a and HCFC-22, are likely the best CH3CCl3 alternatives as atmospheric OH reference gases

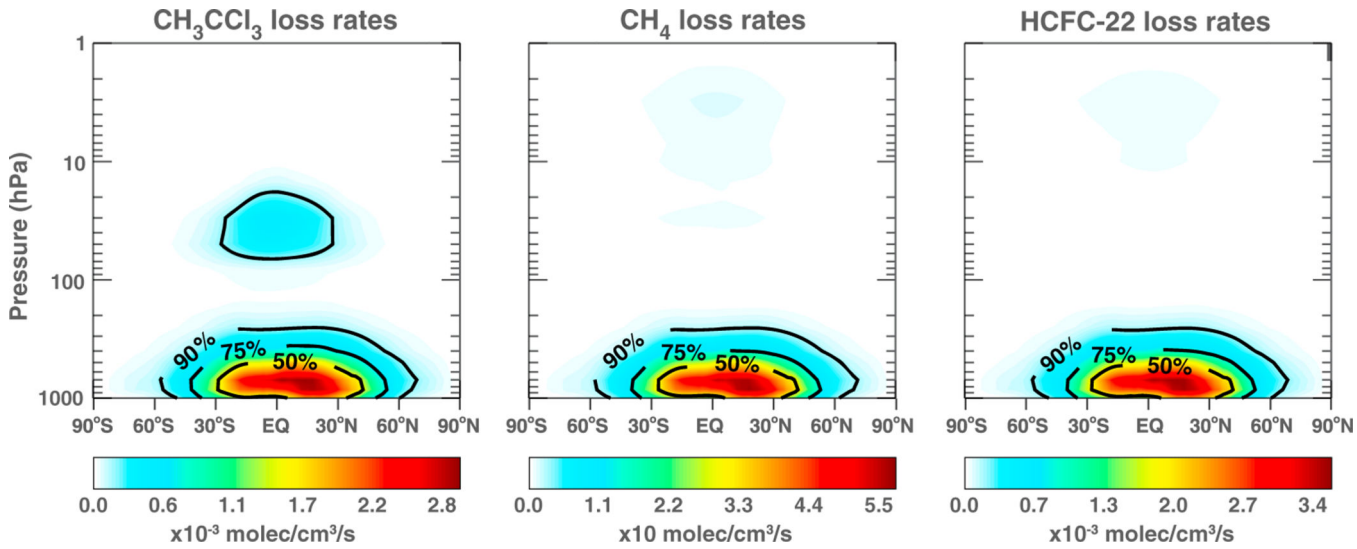

Figure 1.

Latitude-pressure cross sections of zonally integrated annual loss rates of MCF (CH_3CCl_3), CH_4, and HCFC-22 from the WACCM model using the 30 year averaged model output from the 2000 time-slice run, with warm colors indicating larger loss rates. The black contours outline the regions where more than 50%, 75%, and 90% of the globally integrated loss occur.

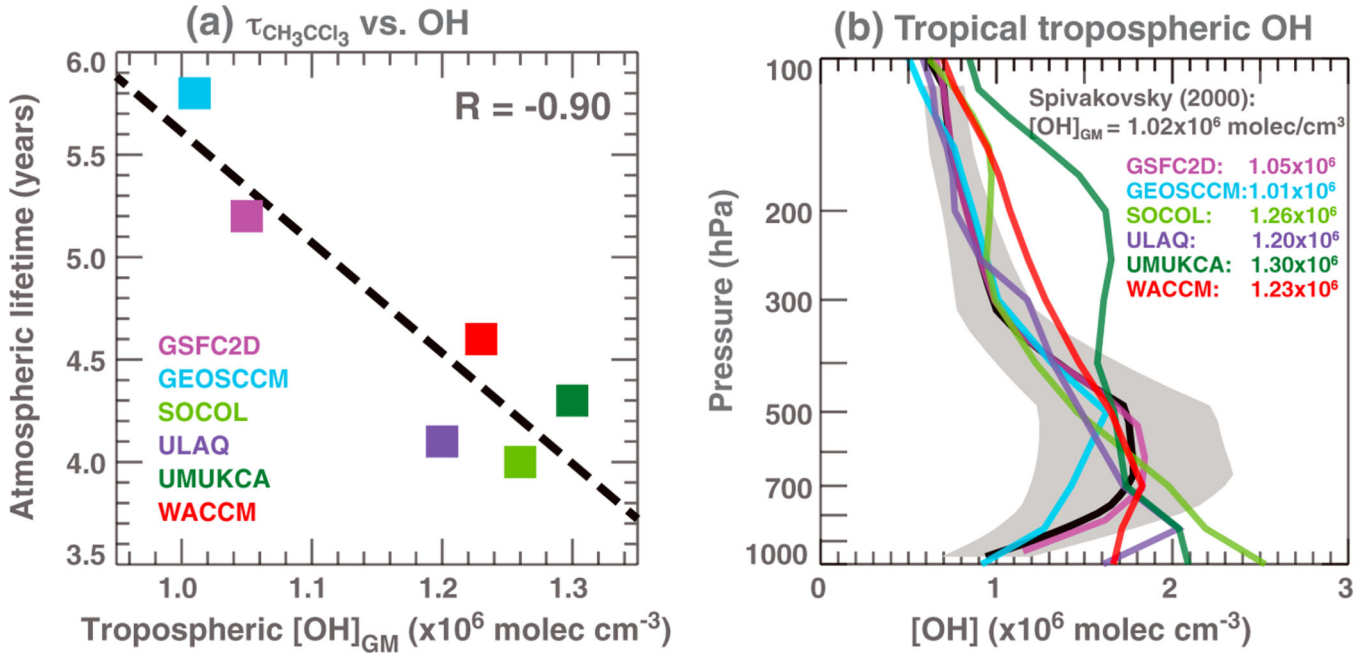

Figure 2.

(a) Modeled steady state atmospheric lifetimes (years) from the TS2000 simulation for CH_3CCl_3 versus mass-weighted tropospheric OH abundance. (b) Comparison of tropical (30°S–30°N) annual mean OH profiles from Spivakovsky et al. (2000) (thick black line with gray shading indicates 1σ spatial and temporal variance in that model) and the models. The global mean OH abundances from Spivakovsky et al. (2000) and those derived from the models ($[OH]_{GM}$; molecules cm^{-3}) are given in the legend. All CCM results are 30 year annual average from the 2000 time-slice simulations.

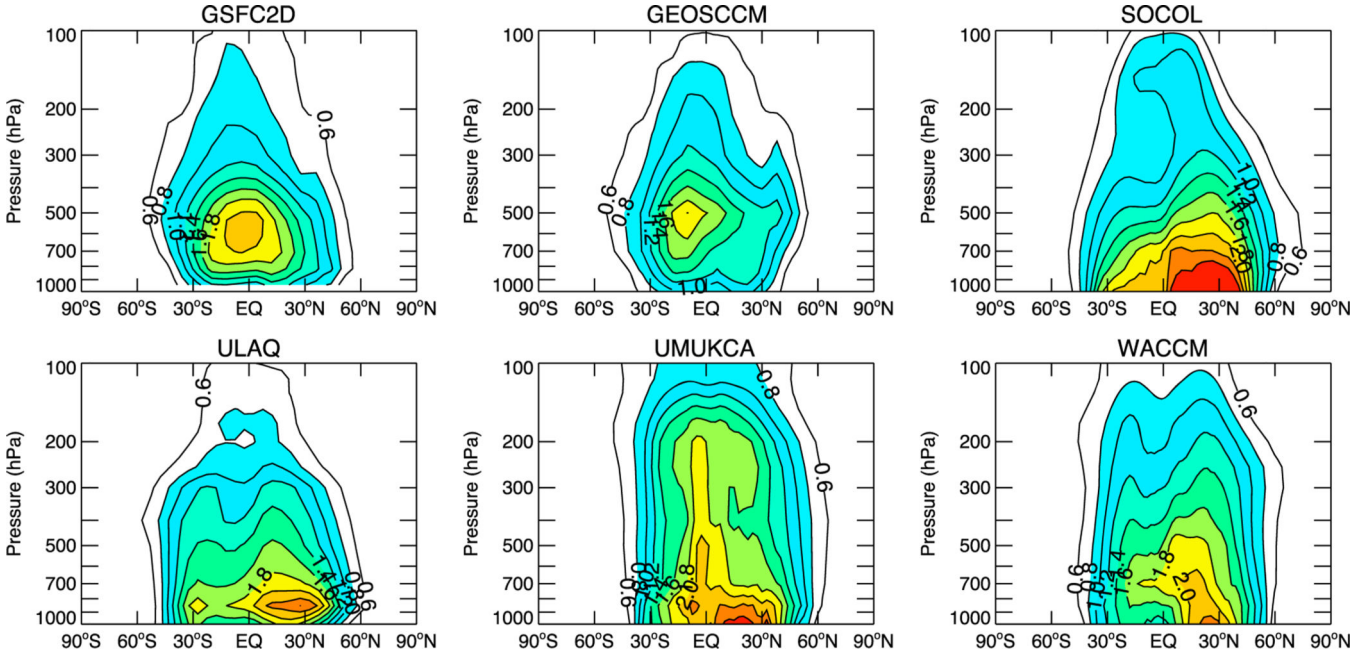

Figure 3.

Comparison of 30 year averaged model zonal annual mean OH ($\times 10^6$ molecules cm^{-3}) from the 2000 time-slice simulation for the GSFC2D, GEOSCCM, SOCOL, ULAQ, UMUKCA, and WACCM models.

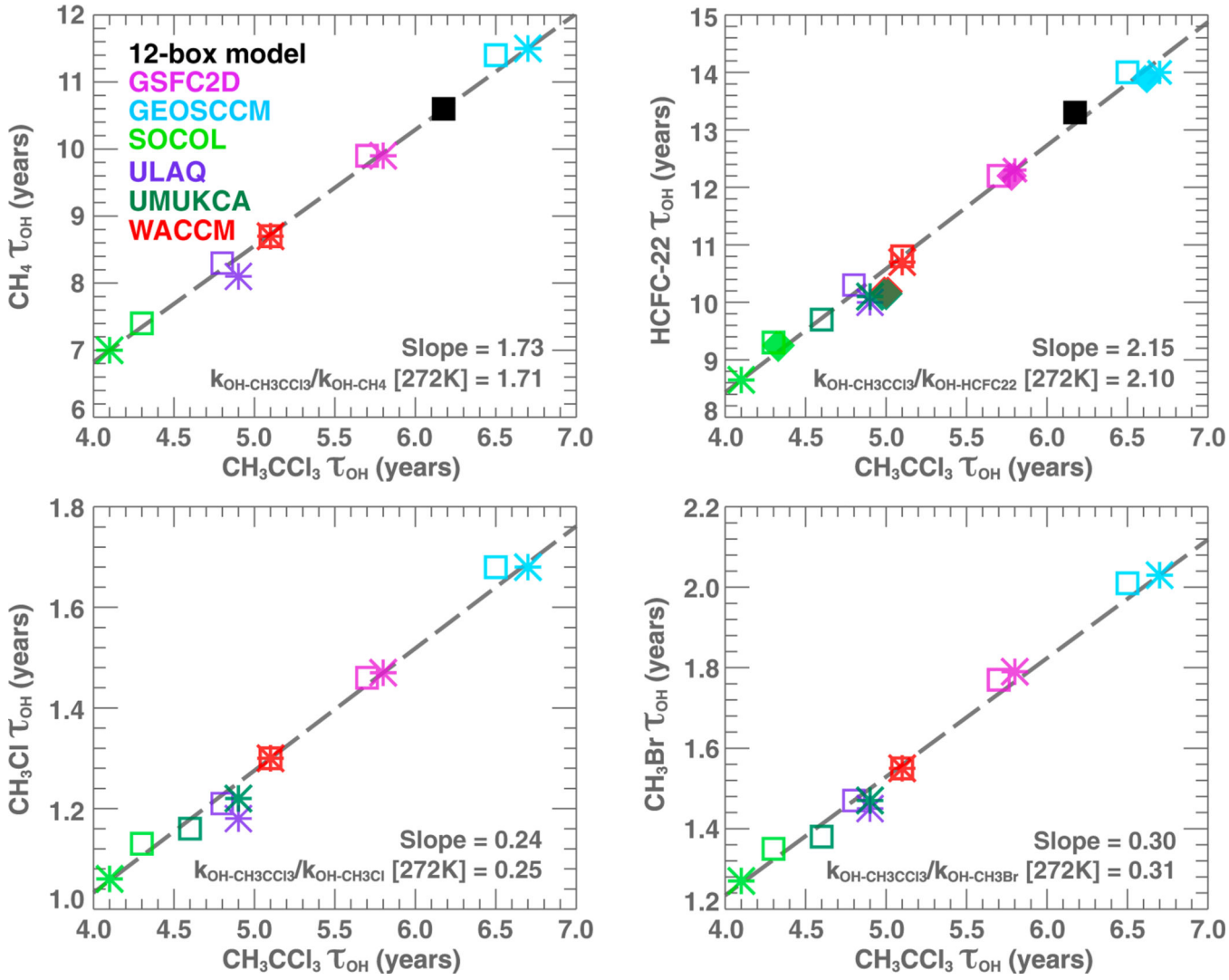

Figure 4.

Modeled τ_{OH} (years) for (a) CH_4, (b) HCFC-22, (c) CH_3Cl, and (d) CH_3Br versus modeled τ_{OH} of MCF. Results shown are the steady state τ_{OH} from the TS2000 simulations (squares) and the transient τ_{OH} in 2000 from the TRANS simulations (asterisks). The τ_{OH} of the FBC tracers from individual models, when available, is also shown (diamonds). The 12-box IM-inferred τ_{OH} for CH_4 and HCFC-22 are shown as well (black filled squares).

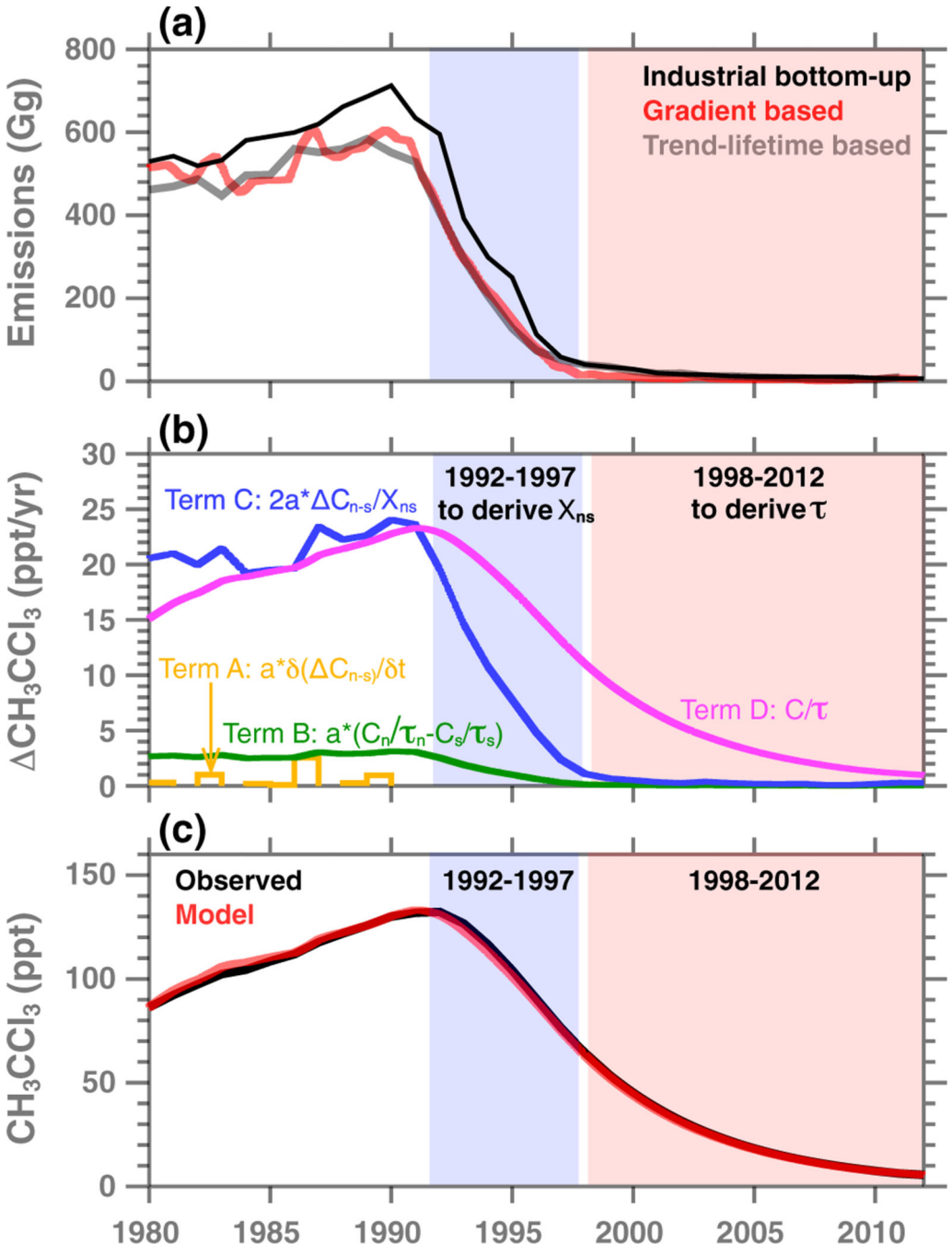

Figure 5.

(a) Comparison of industrial-based bottom-up (black), interhemispheric concentration difference-based (red), and global trend and MCF lifetime-based (gray) emissions during 1980–2012. (b) The contribution of terms A–D in equation (7) to the MCF trend over the same time period. (c) The AGAGE observed (black) and two-box model calculated (red) global mean CH_3CCl_3 mixing ratios during 1980–2012 using the gradient-based emissions derived in Figure 5a.

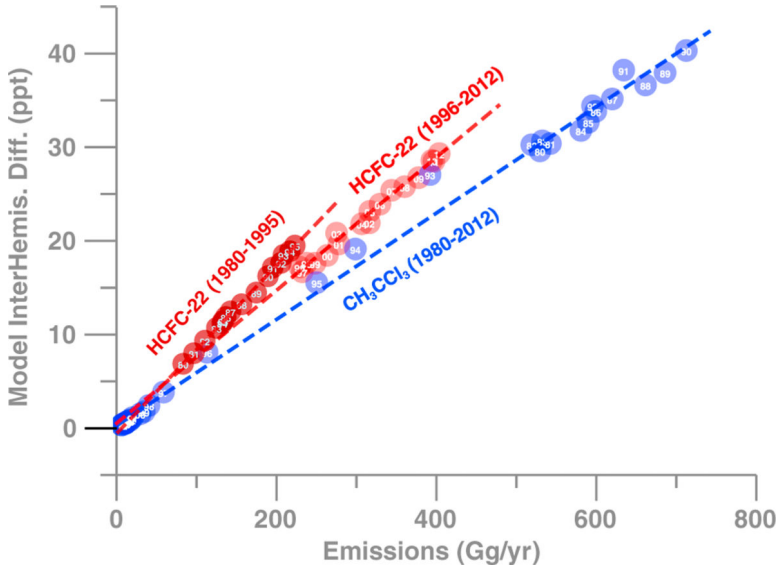

Figure 6.

Correlation of annually averaged model interhemispheric mixing ratio difference, ΔC_{n-s}, for HCFC-22 and CH_3CCl_3 with the annual global emissions used in the model simulation. The linear fit regression lines are shown as dashed lines. Numbers in each circle mark the year of the model results. Different NH emission fraction (F_n) values were used in the GEOSCCM simulation for HCFC-22 for 1980–1995 and 1996–2012. Since the regression slope (af/b in equation (6)) is a function of F_n, the 1980–1995 results fall on a different regression line than the 1996–2012 results.

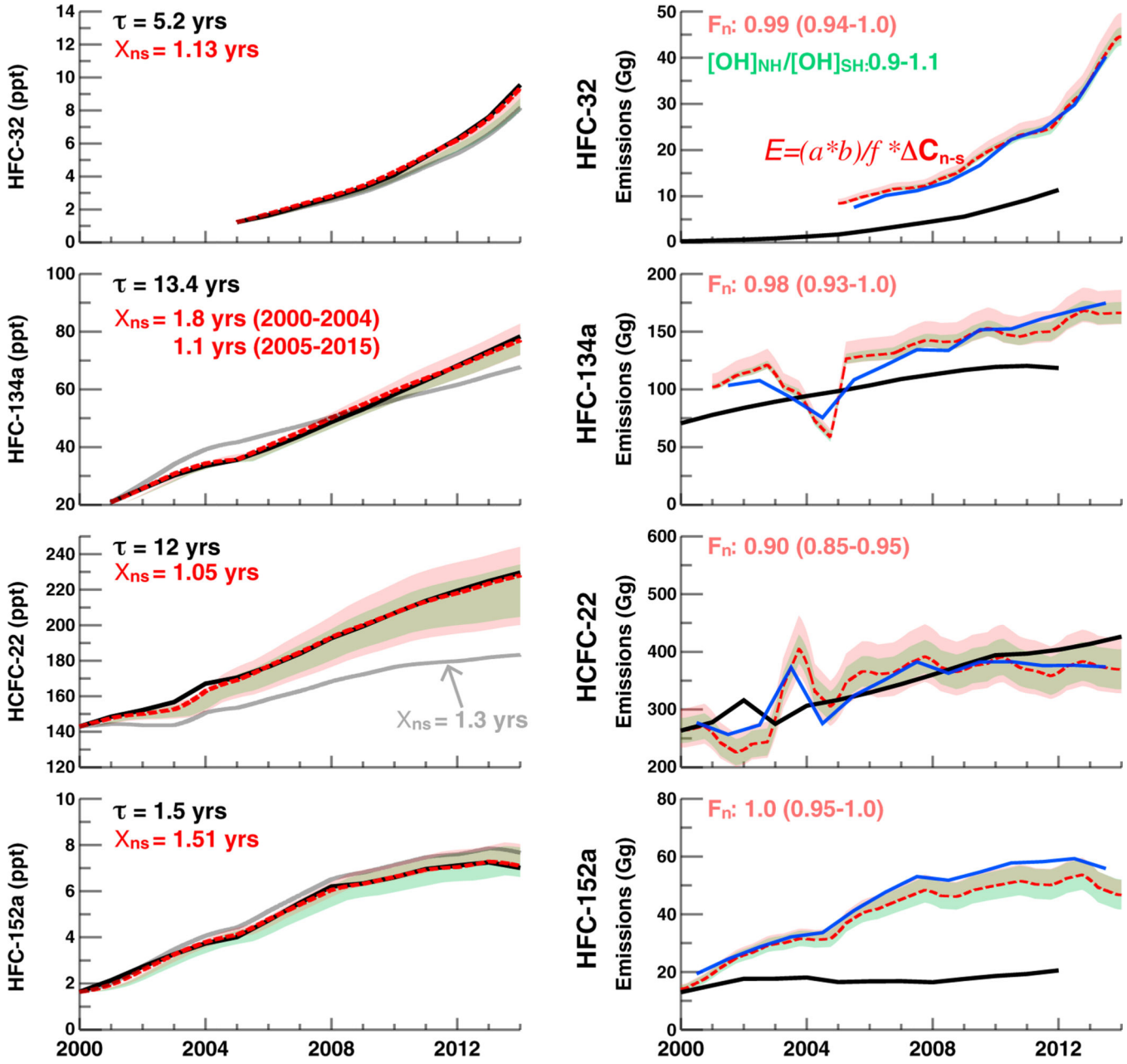

Figure 7.

(left) The two-box model calculated trends for HFC-32, HFC-134a, HCFC-22, and HFC-152a using a MCF-based X_{ns} of 1.3 years (gray lines) and the optimal X_{ns} (dark red dashed lines) that best match the observations (black lines). (right) Comparison of the gradient-based emissions (dark red dashed lines), the trend lifetime-based emissions (blue lines), and the inventory bottom-up emissions from the nonarticle five countries (black lines). Annual mean C, ΔC_{n-s}, $\partial C/\partial t$, and $\partial \Delta C_{n-s}/\partial t$ are calculated using atmospheric observations from the AGAGE network. Annually varying F_n are calculated based on emission inventory reported to UNFCCC (section 4.2). Sensitivity of the simulated surface mixing ratios and gradient-based emissions are also shown to reflect emission uncertainties

in (1) the fraction of global emissions emitted in the NH, F_n (0.05 to +0.05 or unity of 1 whichever is the smallest; light green shading) and (2) NH-SH OH difference (NH/SH ratio of 1 ± 0.1; light red shading).

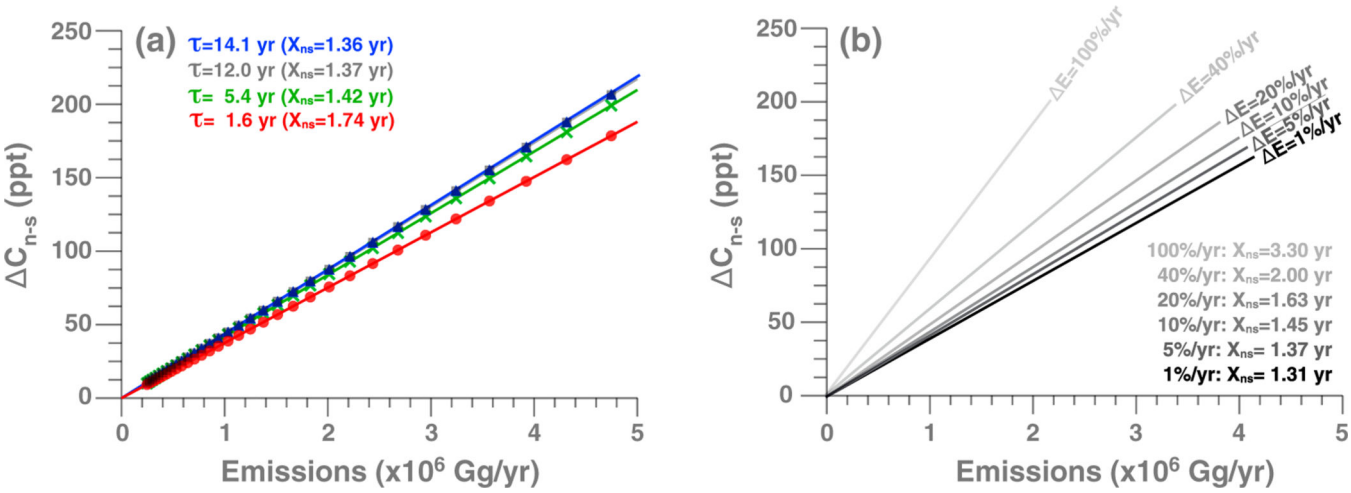

Figure 8.

The modeled annual mean interhemispheric mixing ratio difference (ΔC_{n-s}) versus emissions and its dependence on (a) trace gas lifetime, from 1.6 years to 14.1 years, with a 5%/yr increase in emissions and (b) rate of change in emissions, from an increase of 1%/yr to 100%/yr for a HCFC-22 like tracer with a lifetime of 12 years, based on idealized tracer sensitivity simulations conducted using the GSFC2D model (see text for details). The symbols represent the values for individual years, and the lines show the regression slopes for each sensitivity simulation. The X_{ns} values derived from these GSFC2D model results for each lifetime/emission scenario are also included.

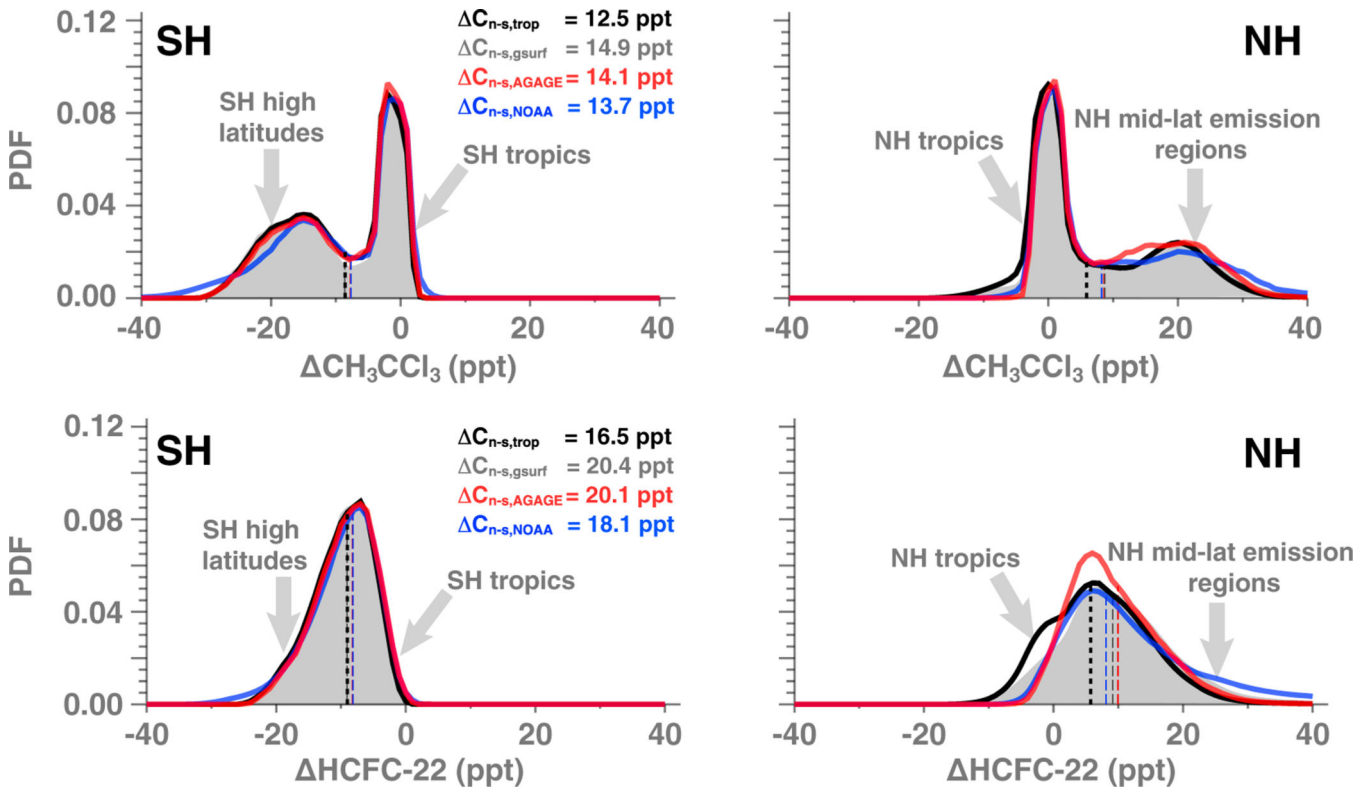

Figure 9.

The model probability distribution function of the (left) SH and (right) NH detrended mixing ratio anomalies (with respect to global mean values) for CH_3CCl_3 and HCFC-22 during 1980–2014. ΔC_{n-s} calculated using all global surface grids ($\Delta C_{n-s,\mathrm{gsurf}}$; gray shading for distribution probability and thin gray dashed lines for area-weighted hemispheric mean anomaly) differ from those calculated using the modeled values sampled at the AGAGE stations (thick red lines for distribution probability and red dashed lines for hemispheric mean) and the NOAA-GMD stations (thick blue lines for distribution probability and blue dashed lines for hemispheric mean). Station-based values are interpolated to all latitudes, from 90°S to 90°N, for full global representation. The modeled distribution probability (thick black lines), hemispheric means (black dashed lines), and $\Delta C_{n-s,\mathrm{trop}}$ calculated using all grid cell results below 500 hPa are also shown.

Table 1

Global Mean Tropospheric OH Concentrations ($\times 10^6$ molecules/cm^3, Mass-Weighted)

$[OH]_{GM}$	**Published values**[a]	**GSFC2D**	**GEOSCCM**	**SOCOL**	**ULAQ**	**UMUKCA**	**WACCM**
2000s (below 100 hPa)	0.7–1.24	0.91	0.87	1.07	0.99	1.22	1.07
2000s (below 200 hPa)	0.94–1.0	1.05	1.01	1.26	1.20	1.30	1.23

Note. Results for the 2000s and 2100s are calculated using the final 10 years of model output from the TS2000 simulations, and results for the 1960s are 10 year averages between 1960 and 1969 from the TRANS simulations.

[a]The published values of mass-weighted OH concentration adapted from Lawrence et al. (2001).

Table 2

Atmospheric Abundances and Observed Global Trends of MCF, HCFCs, and HFCs From the AGAGE Network

		Lifetime[a] (years)									
Name	**Formula**	τ	τ_{OH}	$\tau_{O(1D)}$	τ_{hv}	**Abundance[b] in 2012 (ppt)**	**Growth rate (ppt/yr)**	**Term A** $a \cdot \frac{\partial \Delta C_{n-s}}{\partial t}$ **(ppt/yr)**	**Term B** $a \cdot (\frac{C_n}{\tau_n} - \frac{C_s}{\tau_s})$ **(ppt/yr)**	**Term C** $a \cdot \frac{2\Delta C_{n-s}}{X_{ns}}$ **(ppt/yr)**	**Term D** $-\frac{C_g}{\tau}$ **(ppt/yr)**
MCF (1992–1997)	CH_3CCl_3	5.0	6.0		46	5.5	−10.0	− 2.1 (7%)	1.1 (4%)	8.4 (29%)	−17.4 (60%)
MCF (1998–2014)							−3.7	−0.04 (1%)	0.04 (1%)	0.3 (7%)	−4.0 (91%)
HCFC-22	**$CHClF_2$**	**12**	**12.1**	**733**		**219.2**	**1.9**	**−0.2** (1%)	**0.8** (2%)	**13.4** (45%)	**−15.7** (52%)
HCFC-141b	CH_3CCl_2F	9.4	10.3		108	22.5	0.5	0.04 (1%)	0.1 (3%)	1.7 (44%)	−1.9 (52%)
HCFC-142b	CH_3CClF_2	18	18.8	505		21.9	0.5	−0.08 (4%)	0.05 (2%)	1.3 (56%)	−1.1 (46%)
HFC-23	CHF_3	228	228			25.0	0.8	0.03 (4%)	0.002 (0%)	0.6 (83%)	−0.1 (13%)
HFC-32	**CH_2F_2**	**5.4**	**5.4**			**6.3**	**1.0**	**0.2** (7%)	**0.2** (7%)	**1.3** (54%)	**−0.7** (32%)
HFC-125	CHF_2CF_3	31	33	700		11.2	1.2	0.1 (6%)	0.03 (2%)	1.3 (75%)	−0.3 (17%)
HFC-134a	**CH_2FCF_3**	**14**	**14.1**	**3010**		**67.8**	**4.4**	**0.1** (1%)	**0.3** (3%)	**6.4** (60%)	**−3.9** (36%)
HFC-143a	CH_3CF_3	51	53.3	1180		13.4	1.1	0.04 (2%)	0.01 (1%)	1.1 (82%)	−0.2 (15%)
HFC-152a	**CH_3CHF_2**	**1.6**	**1.6**			**6.9**	**0.2**	**0.06** (1%)	**1.5** (18%)	**3.5** (41%)	**−3.5** (40%)

Note. The current best estimate lifetimes and partial lifetimes of these gases from SPARC (2013) and Carpenter et al. (2014) are also listed. An assessment of the relative contributions (ppt/yr; as well as the percentages) of the four terms (equation (7)) to the observed global trend (annual mean values) during 2005–2014 is also shown. For these results, we use the optimal estimate annual F_n described in section 3.2.1 and X_{ns} described in section 3.2.2 and assume that $\tau_n = \tau_s = \tau$. Note that the percentages are calculated with respect to the sum of the absolute magnitudes of all four terms. Our recommended best MCF alternative reference gases are highlighted in bold, the two gases for global OH in blue and the two for hemispheric OH in light blue.

[a] τ is the total lifetime due to all removal processes, and all partial lifetimes are calculated using global integrated losses throughout the atmosphere.

[b] Surface abundance in 2012 based on AGAGE measurements (Carpenter et al., 2014).

Table 3

A Detailed List of Atmospheric Abundance, Kinetic Rate Uncertainty, Industrial Usage, and the Associated Banking Times for the Four MCF Alternatives

Name	Information provided	Abundance 2012 (ppt)	$f(272\text{K})$ [a]	Usage and banking times	
HCFC-22	$[OH]_{NH}$ and $[OH]_{SH}$	219.2	1.10	open-cell foam blowing refrigeration/air conditioning closed-cell foam blowing	Short (<1 years) Medium (1–10 years) Long (>10 years)
HFC-32	$[OH]_{GM}$ and τ_{OH}	6.3	1.10	Refrigeration/air conditioning	Medium (1–10 years)
HFC-134a	$[OH]_{GM}$ and τ_{OH}	67.8	1.14	Aerosol propellant, open-cell foam blowing refrigeration/air conditioning closed-cell foam blowing	Short (<1 year) Short (<1 year) Medium (1–10 years) Long (>10 years)
HFC-152a	$[OH]_{NH}$ and $[OH]_{SH}$ and [OH] seasonality	6.9	1.07	Aerosol propellant and open-cell foam blowing	Short (<1 year) Short (<1 year)

[a] $f(272\ \text{K})$ is the 1σ uncertainty factor for k-OH rate constant at 272 K, calculated using the following formula: $f(272K) = f(298K) \cdot \exp(|g(\frac{1}{272} - \frac{1}{298})|)$, where $f(298\ \text{K})$ is the rate constant uncertainty at 298 K and g is the quantity used with $f(272\ \text{K})$ to calculate the uncertainty at different temperatures other than 298 K (SPARC, 2013).